Reliability and Power Degradation Rates of PERC Modules Using Differentiated Packaging Strategies and Characterization Tools

Project Title	**Reliability and Power Degradation Rates of PERC Modules Using Differentiated Packaging Strategies and Characterization Tools**
Report	**Research Performance Progress Report Part 1 (RPPR-1)**
Project Period	(10/01/2017 – 09/30/2020)
Budget Period	(10/01/19 – 09/30/2020)
Reporting Period	(09/30/20 – 12/30/20)
Reporting Frequency	Semi-Annually
Submission Date	01/30/2021
Award Number	**DE-EE-0008172**
Recipient	**Case Western Reserve University**
Address	10900 Euclid Avenue Cleveland, OH 44106-7204
Website	SDLE Research Center
Project Team	**Case Western Reserve University**
Collaboration With	**Univ. of Central Florida, Univ. of Connecticut DuPont, Cybrid, Canadian Solar Inc.**
Principal Investigator	**Roger H. French, Kyocera Professor**
Phone:	216-368-3655
Email	rxf131@case.edu
Business Contact	**Jonathan Steirer, SDLE Operations Manager**
Phone	484-634-2478
Email	jws227@case.edu
HQ Tech Manager	**Marie Mapes**
HQ Project Officer:	**Christopher Anderson**
GO Grant Specialist:	**Fania Barwick**
GO Contracting Officer:	**Diana Bobo**

Signature Date

CASE SCHOOL OF ENGINEERING SDLE
CASE WESTERN RESERVE UNIVERSITY

Information from Statement of Project Objectives (SOPO)

The reliability, durability and lifetime performance of passivated emitter, rear cell (PERC) modules used in real-world PV power plants is a critical challenge underlying the rapid adoption and bankability of these PERC cells, whose high efficiency help reduce the levelized cost of electricity (LCOE). We propose a degradation-science study of PERC module degradation pathways, benchmarking them relative to known degradation mechanisms and pathways of the incumbent aluminum back surface field (Al-BSF) modules exposed to real-world and accelerated exposure conditions. To achieve this objective, we propose three project goals:

Goal 1. Develop PERC module degradation pathway network models, benchmarking against Al-BSF, using full- and mini-modules under accelerated and real-world exposure conditions. This will include mono- and multi-crystalline PERC and half-cell PERC modules.

Goal 2. Quantify interactions between PERC cells and module packaging strategies using mini- modules fabricated with ethylene vinyl acetate (EVA), thermoplastic olefin (TPO), and polyolefin elastomer (POE) encapsulants and backsheets with different vapor transmission rates (VTR), so as to define packaging capable of lowering power degradation rates (R_d) to 0.2%/yr. and extending module lifetime towards 50 years.

Goal 3. Utilize novel characterization methods to identify PERC specific degradation modes and their characteristic signatures, so as to define and deploy field survey and field deployable diagnostics for PERC-based power plants.

Life-stress prediction models are based upon accelerated conditions assuming a single dominant failure mode. Outdoor testing is the best method of ensuring that high accelerated aging is not inducing damage, yet the slower degradation processes require much more sensitive probes of carrier dynamics. Our methods rely heavily on modern statistical modeling/machine learning for hypothesis testing (Goal 1 / Task 4). Degradation pathway models from accelerated exposures on mini-modules will be validated against models built from power plant data and past accelerated exposures on full-size modules (Goal 1 / Task 1). Our models will be expanded to include results from high-resolution characterization tools (Goal 3 / Task 3), which provide data relating variables to performance loss. The variables include the typical stressors (high heat, humidity, light intensity) but also data from mechanistic and performance evaluations for a complete multivariate network model predicting performance and improvement schemes. Our research will demonstrate the feasibility of this technique as an electronic-only method for determining degradation phenomena in a fast and extremely sensitive manner. We will also demonstrate feasibility of a field-capable measurement tool. The analysis of degradation mechanisms utilizes the network modeling approach to understand module-wide performance and statistically significant interactions. It is known that hydrolysis of ethylene-vinyl-acetate encapsulants results in acetic acid exposed to the front-side of the cells. However, the effects of an acidic environment on thin film oxides over decades is not well understood as to be predictable, particularly as it affects surface recombination velocities in PERC PV. Alternative non-EVA encapsulants will be tested alongside backsheets with varying VTRs to optimize packaging of PERC modules for extended lifetime. These encapsulants (POE and TPO) are alternatives to EVA and may change degradation rates and mechanisms by reducing metallization corrosion and reduce potential induced degradation.

In this program we will concentrate on the utility of semiconductor characterization techniques to enhance the sensitivity of the determination of performance loss. These methods are not conventionally utilized in lifetime studies, but are fundamentally related to the measurement and understanding of carrier recombination within the semiconductor. Additionally, current vs voltage and transient loss response measurements will provide the system series resistance external to the cells. This methodology then focuses on validating sensitive measures of PV module performance that are external, electronic measures, and field- capable, such as time-resolved EL. At the end of this project, we aim to have degradation pathway models for mono- and multi- crystalline PERC full-size modules as a function of their packaging materials (encapsulant and backsheet). We also expect to have developed a field deployable module-level characterization method to monitor performance and degradation, incorporated into our $< Stressor|Mechanism|Response >$ models diagnose degradation mechanisms.

Contents

1 Executive summary

1.1 SDLE Research Center at Case Western Reserve University

SDLE has completed the mDH + FS exposure of minimodules and is continues collection additional outdoor data. We have been focused on the analysis of the collected data from these exposures, with a submission to PVSC and future paper regarding the results of the minimodule accelerated tests.

1.2 University of Central Florida

UCFs primary focus has been the sectioning of modules and minimodules and the analysis there of, in partnership with UConn. Materials characterization on full sized modules demonstrated the role of Pb and Sn in degradation of cell interconnects.

1.3 University of Connecticut

Focused Ion Beam etching and SEM with EDS mapping showed the complex role of the glass fritted pastes and Sn in migration and performance degradation.

1.4 Canadian Solar

In addition to provide the state of the art cells and modules studied in the project, CSI also developed the PERC cell stabilization processes used in the project. They also provided the samples and exposures to study the durability of cell passivation layers used in mono- and bi-facial PERC cells. This work focused on the importance of understanding PERC specific degradation mechanisms, and the reliability of differing passivation layers to UV degradation. This study found that with appropriate cell stabilization procedures, PERC cells do not show greater degradation under UV exposure.

1.5 Key findings

- PERC vs. Al-BSF performance

  PERC cells, as expected, showed better performance than Al-BSF cells. In addition PERC cells showed better reliability, with bifacial PERC showing the best reliability, as summarized in Figure 7.

- Performance based on packaging

  Due to the improved reliability of bifacial PERC cells, there has been interest in the use of white EVA, to make monofacial modules that use bifacial cells, with the back of cell white EVA scattering light back into the PERC cell. While this concept is still sensible. The strong corrosion arising from one of the two white EVA encapsulants we studied, suggest more work and caution is required.

- Metallization corrosion degradation

  There is a clear trend of higher risk of metallization corrosion in white EVA encapsulated samples, particularly with Al-BSF cells. It is also observed that different white EVA suppliers show vastly different performance. It is currently unknown what the difference between the two suppliers is, however we are currently investigating the TiO_2 particles in each material to assess any variations between them. As TiO_2 is known to produce free radicals through photo-excitation, the quality of the TiO_2 may have a strong influence on the stability of the EVA and subsequently the module as a whole.

- Transfer to PERC cells

  PERC cells, both mono- and multi-crystalline silicon, show better reliability when they are bifacial cells. Our theory is that the reduced bowing stress, and symettry of the bifacial cells plays a role in this.

1.6 State of the art advancement

- Project outputs and publications

  This project produced 20 conference presentations, proceedings and journal articles.

- R packages

  As part of this project, we developed the PVplr R package of code, to determine the Performance Loss Rate of PV systems.

- Datasets/IEA-PVPS

  The PVplr package and DOE Baseline systems were used in the 3 year PLR determination project undertaken by French as Task Lead, in the work of the IEA-PVPS Task 13 on Reliability and Performance

Narrative Report and Update:

Here we describe in more detail our primary workflows during the extension period of the project.

2 Project results and discussion

2.1 Task 1

Time-series I-V data for full-sized modules subjected to outdoor fielding and indoor accelerated exposures will be provided by a PV manufacturer such as Canadian Solar. These datasets may also include EL images or other characterization data that will help to identify mechanisms of power loss. We will also obtain full-size modules to be fielded at our SunFarm in Cleveland, OH, and seek additional real-world power plant data for fielded PERC modules. The data obtained in this task will encompass several variations of full-size modules including Al-BSF and PERC, mono-and multicrystalline cells, half-and full-cells, and different packaging materials, to be compared and modeled throughout the project term.

2.2 Task 2

2-cell mini-modules will be fabricated at the SDLE Research Center at CWRU using mono-crystalline cells, multi- crystalline cells, and packaging materials from a company such as Cybrid Technologies. These mini-modules will incorporate various cell and packaging strategies, including Al-BSF and PERC cells, 2 different encapsulants, 3 different backsheets, and full-and half-cells. The mini-modules will undergo outdoor fielding, as well as accelerated exposures.

2.3 Task 3

The modules and mini-modules exposed in Tasks 1 & 2 will be characterized using methods listed in the Technical Scope Summary. Our module-level characterizations range from traditional evaluations such as I-V curve tracing, to cutting-edge methods like EQE+R and Suns-Voc which are novel in the study of PV degradation. By employing these characterizations on modules at predetermined points in the exposure process, we will generate diverse time-series datastreams that include both degradation mechanisms and module performance responses. We will expand tool capabilities from cell-level to module-level, while also exploring field-deployable techniques for real-world degradation detection and tracking. Destructive testing with pcAFM will give insight to the nanoscale behavior of cells, and confirm diagnoses from module-level characterizations.

2.4 Task 4

Using the existing data analytics framework at CWRU, we will build $< Stressor|Response >$ & $< Stressor|Mechanism|Response >$ models from the time-series datastreams generated in Tasks 1, 2, & 3. These models will be used to quantify, predict, and compare degradation rates of various types of modules and mini-modules to rank-order the employed technologies for commercial viability. $< S|M|R >$ modeling will utilize mechanistic characterizations completed in Task 3 to quantify and rank PERC-specific degradation pathways.

2.5 End of project milestones

3 Project Progress Over Full Term & Extension Period

As of now all project tasks have been completed with the exception of the end of project tasks due at the end of the extension period. Given the large numbers of samples and characterizations performed in this project, the extension period has been of great benefit in pursuing notable findings from previous project research. In this section we will discuss the outcomes of the work in the extension.

3.1 SDLE

SDLE has completed the mDH + FS exposure of minimodules and is continues collection additional outdoor data. We have been focused on the analysis of the collected data from these exposures, with a submission to PVSC and future paper regarding the results of the minimodule accelerated tests.

Analysis of Outdoor Data

As we have worked through multiple sets of outdoor data between mini and full sized modules as well as industrial scale plants, we have built a code base design to extract PLR results from time-series PV data. We have discussed this code frequently in past reports, however we recently built a publicly available R package uploaded to CRAN for use by anyone.[1]

There are two outdoor data sources we are currently monitoring from sites at SDLE and from CSI. CSI has been the predominant source of full-sized module measurements, both indoors and outdoors. In the past we have reported extensively on the outdoor exposed modules with periodic indoor measurements, while there are no current updates to this data at 3.6 years of exposure, we expect a new update of the past 8 months of exposure soon. This data source has been the best way to evaluate outdoor PLR values, being the data with the most historical data. This final data addition will push this past 4 year for the oldest modules. In addition to the indoor measurements, CSI has recently provided a large dataset consisting of in situ measurements of the modules during operation, including a set of modules with time-series I-V tracing. These dataset are either new or significant temporal additions to existing data so we will be analyzing this data as an additional source of outdoor information.

The other data set being extended are the SDLE outdoor minimodules. Minimodule variants are from the first round of minimodules, with multi Al-BSF and mono PERC cells. Encapsulant variants include UV cutoff EVA and POE, with KPx and PPf backsheets. A summary of the mini-modules and their packaging combinations is given in Table 1. The modules have recently reached 28 months of exposure.

Table 1: Characteristics of 16 outdoor mini-modules.

	Sample	Cell	Back Encap	Backsheet
1	sa42615	PERCgen1	EVA/C11	KPX
2	sa42616	PERCgen1	EVA/C11	KPX
3	sa42625	Al-BSF	EVA/C11	KPX
4	sa42626	Al-BSF	EVA/C11	KPX
5	sa42638	PERCgen1	POE/C22	KPX
6	sa42639	PERCgen1	POE/C22	KPX
7	sa42645	Al-BSF	POE/C22	KPX
8	sa42646	Al-BSF	POE/C22	KPX
9	sa42697	PERCgen1	EVA/C11	PPf (295B)
10	sa42698	PERCgen1	EVA/C11	PPf (295B)
11	sa42708	Al-BSF	EVA/C11	PPf (295B)
12	sa42709	Al-BSF	EVA/C11	PPf (295B)
13	sa42718	PERCgen1	POE/C22	PPf (295B)
14	sa42719	PERCgen1	POE/C22	PPf (295B)
15	sa42728	Al-BSF	POE/C22	PPf (295B)
16	sa42729	Al-BSF	POE/C22	PPf (295B)

The time-series features a number of loss events, the largest of which being a several month dark period when a load unit was broken and had to be shipped out for replacement. As such, extensions of these datasets helps to alleviate the influence of missingness. An example of a performance ratio time-series is shown in Fig. 1, with the gap from the load unit failure appearing at the beginning.

As a progression towards the end of project milestone we are applying indoor characterization techniques to outdoor data. In this case the $Suns$-V_{OC} loss mechanisms are extracted from the outdoor data sets by building pseudo I-V curves from the voltage, temperature, and irradiance data. Comparing the pseudo I-V curves to real I-V curves shows where losses in performance are occurring. A demonstration of the loss mechanisms is shown in Fig. 2. There is a large amount of noise in the uniform current loss, suggesting discrepancies between I_{SC} and measured irradiance. The more stable mechanisms, recombination and R_S loss show periods of greater power loss but only for given periods, returning to near zero afterwards. This would suggest we are capturing loss from events such as soiling or partial shading instead of consistent degradation. Overall, there is not much observable and consistent change over time for the minimodules, indicating a low amount of degradation. This is consistent with PLR results for the minimodules, with confidence intervals showing strong overlaps with 0. We will continue to monitor and collect data from these minimodules as we move forward to see if we can find consistent loss mechanisms.

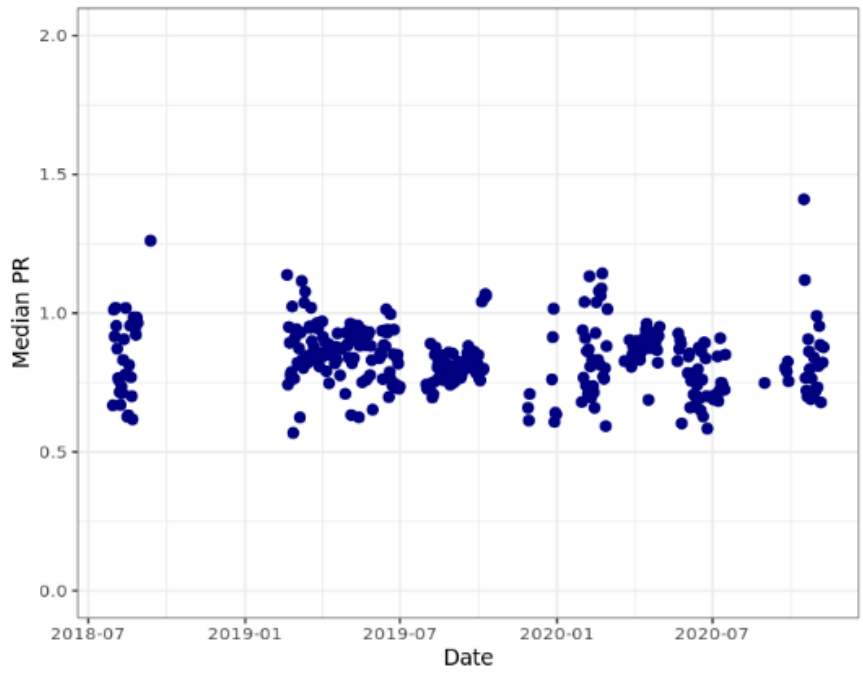

Figure 1: Weekly average performance ratio from an outdoor mini-module.

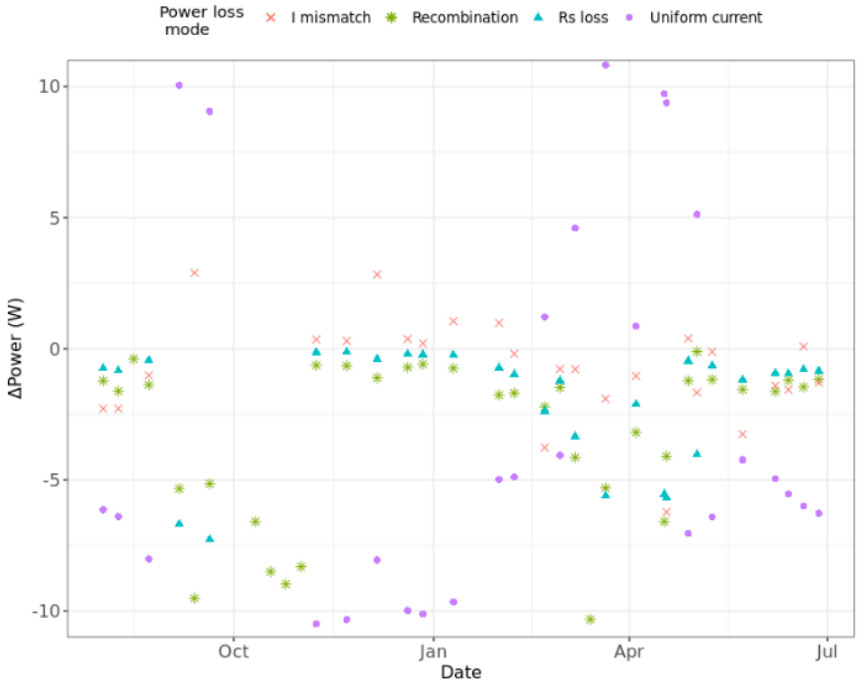

Figure 2: Power loss mechanisms from outdoor $Suns$-V_{OC} analysis.

mDH + FS Exposure & PVSC 2021 Submission

The modified damp heat with full spectrum light (mDH+FS) exposure has completed its intended time of at least 3500 hours, and was extended to 9 total steps totaling 4536 hours of exposure.

The exposure extension was done as the mDH+FS splits time between the mDH and FS sections of the exposure at a 2:1 ratio. A visual representation of the exposure is given in Figure 3, with both total exposure and individual mDH and FS exposure.

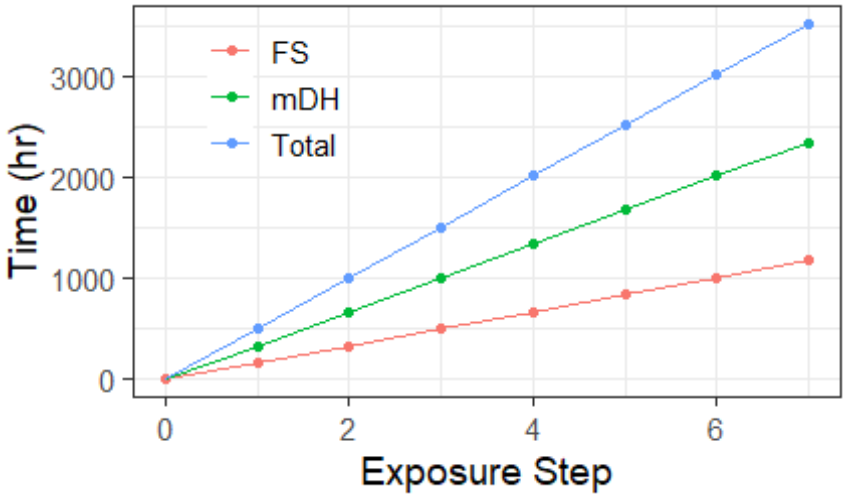

Figure 3: mDH + FS accelerated exposure timeline split between mDH and full spectrum. Mini-modules receive a 2:1 dose of mDH to FS exposure per step.

When comparing to the mDH exposure, the mDH+FS showed much less degradation at nearly the same run time, however, mDH+FS has a lower cumulative mDH dose, making it less aggressive. Two additional mDH+FS steps were performed to induce more degradation bring the total lifecycles of the modules closer to those in mDH. This would provide a better comparison between the exposures. The current progress on the mini-module exposure have been submitted as a PVSC-48 evaluation abstract.

Testing samples are eight half-cell minimodules with the cells arranged in half-cell pairs in a two by two configuration. The cells are wired with each half in parallel, creating two parallel sets of four half-cells in series. This configuration gives similar V_{OC} and I_{sc} magnitudes to four full cells in series. Measurements can be made on the full minimodule as well as measurements of the individual cell pairs. As the half cell pairs are in series they have approximately double the V_{OC} and half the I_{sc} of a typical full cell measurement.

The minimodules are produced with the same methods and materials as commercial full-sized modules but at a smaller scale which allows for a greater sample pool and more variety in packaging material. There are three types of silicon cells used; multicrystalline Al-BSF and mono and multicrystalline bifacial PERC. Encapsulant variety includes EVA and POE with UV cutoff and white rear side variations of both. For the white EVA samples there are two different suppliers, denoted as supplier 1 and supplier 2 for anonymity. All of the other encapsulants have the same supplier. All of the samples have the same KPf backsheet.

A summary of all the material combinations for each of the two exposures is given in Table 2.

The samples are divided between two accelerated exposures, modified damp heat (mDH) and modified damp heat with full spectrum light (mDH+FS). The exposures feature a modification of the well known damp heat exposure in that it is run at a lower temperature of $80\ ^oC$ as opposed to the usual $85\ ^oC$. Damp heat (DH) is often criticized as being unrepresentative of real-world

Table 2: Number of minimodules of each cell and encapsulant type per exposure. Individual minimodules can produce multiple data through cell level measurements.

Cell	Rear encap.	mDH count	mDH FS count
multi Al-BSF	White EVA supp. 1	3	1
	White EVA supp. 2	0	1
	White POE	2	2
	UV cutoff EVA	0	1
	UV cutoff POE	0	1
mono PERC	White EVA supp. 1	3	1
	White EVA supp. 2	1	1
	White POE	3	2
	UV cutoff EVA	1	1
	UV cutoff POE	1	1
multi PERC	White EVA supp. 1	3	2
	White EVA supp. 2	1	1
	White POE	2	2
	UV cutoff EVA	1	1
	UV cutoff POE	1	1

degradation and inducing degradation mechanisms that are not commonly observed in fielded modules. In order to better match outdoor exposure conditions we have lowered the temperature to below the glass transition temperature of PET (a common material in backsheets), which occurs below $85\ ^oC$. It has been observed that DH does induces a crystallinity transition in PET that mDH exposure does not [2]. Additionally we have added a light component to one of the exposures, where the minimodules split time between the mDH and a full spectrum light chamber. Given the known susceptibility of PERC cells to LID or LeTID, light exposure is important in any comparison between PERC and Al-BSF cells.

The mDH exposure is run in seven step increments of 528 hours for a total of 3696 hours. At each point measurements are taken and the exposure is continued. The mDH+FS exposure splits time between the mDH and light chambers in a 2-1 ratio. Each step is 504 hours which equates to 336 hours of mDH and 168 hours of FS per step. In total nine steps are run, for a total of 3024 hours mDH and 1512 FS exposure.

At each step the minimodules are measured with both multi-sun I-V and EL/PL measurements. The I-V curves are measured using a Spire solar simulator at 1-sun, 0.5-suns, and 0.25 suns. Measurements are taken at both the full minimodule and cell level, totaling to five measurements per module.

In all cases the predominant degradation mechanism observed what metallization corrosion, as is expected in damp heat. This was confirmed both visually with EL imaging as well as series resistance increases and I_{sc} drops corresponding to P_{mp} losses in the I-V results. There are 15 unique groups of samples when comparing the degradation performance; three cell types and five encapsulant as we treat the white EVA from different suppliers as distinct. Performance between samples is compared based on the models fitted to the trend of the power divided by initial power to account for nameplate variations and cell vs. module measurements. An example of the data

and their models are shown in Fig. 4, with both linear and piecewise linear fits. The trend in corrosion behavior is an initial stable period followed by a large drop in power and in some cases a period of low power stability afterwards. This trend is not well captured by linear models so piecewise linear models are used instead. The piecewise linear model separates a linear model into two or more linear segments which suddenly change slope at changepoints within the trend. The piecewise linear model is able to capture non-linear trends while providing the high interpretability of a linear model as well a quantitative description of when a sudden change occurs within the model via the calculated changepoints.

From these piecewise linear models we can extract the predicted endpoints of all sample types and compare them quantitatively.

The total fractional loss in P_{mp} based on the piecewise linear models for the mDH exposure are given in Fig. 5. The error bars shown are the 83.4% confidence intervals which indicate a $> 95\%$ confidence in mean difference between two or more distributions when the intervals do not overlap. The mDH exposure induced a significant amount of degradation in the minimodules, with the best performing sample retaining 79.6% of its initial power. The best performing samples for this exposure are the multi PERC cells with UV cutoff encapsulant variants of both EVA and POE. The other samples are lower to a statistically significant amount but they generally cluster together, indicating similar performance. The largest discrepancy is not in the best performing samples, but in the poorest performing ones. All of the supplier 1 white EVA samples show considerable power loss compared to all other samples, losing more than 60% of their initial power in all cases. In particular the Al-BSF white EVA combination shows a high susceptibility to metallization corrosion. At the end of exposure all of the supplier 1 white EVA samples show a similar magnitude, however the Al-BSF samples showed a much earlier initiation of corrosion loss than the other two which saturated towards the end of the exposure while the other two caught up. The other white EVA supplier samples do not show nearly as much corrosion, being much more similar to the other encapsulants.

The power loss results for the mDH+FS Exposure are given in Fig. 6; analogous to the results discussed for mDH. Overall the mDH+FS exposure shows less power loss for most of its samples, with the best performer retaining 97.9% of its initial power. The samples cluster differently than the mDH exposure, with the best performers being both the white and UV cutoff POE samples, followed by the UV cutoff EVA, then the supplier 2 white EVA, then the supplier 1 white EVA which again shows much greater power loss than all of the other samples. The only exception to the is the UV POE/multi PERC combination which show a lower power and also a much greater variance than the other POE samples. These samples gave inconsistent measurements due to wiring problems with some of the cells, which gave lower than usual power readings. This discrepancy between cells both reduced the performance and increased the confidence intervals, but this was more due to faults within the samples not metallization corrosion. Again it is observed that the supplier 1 white EVA samples show a much greater amount of corrosion, in particular for the white EVA/Al-BSF combination. The Supplier 2 white EVA samples are more stable but the supplier 2/Al-BSF samples is beginning to show a more rapid decline compared to the other samples, but not the the extent of supplier 1.

In both exposures there is a clear trend of higher risk of metallization corrosion in white EVA encapsulated samples, particularly with Al-BSF cells. It is also observed that different white EVA suppliers show vastly different performance. It is currently unknown what the difference between the two supplier is, however we are currently investigating the TiO_2 particles in each material to

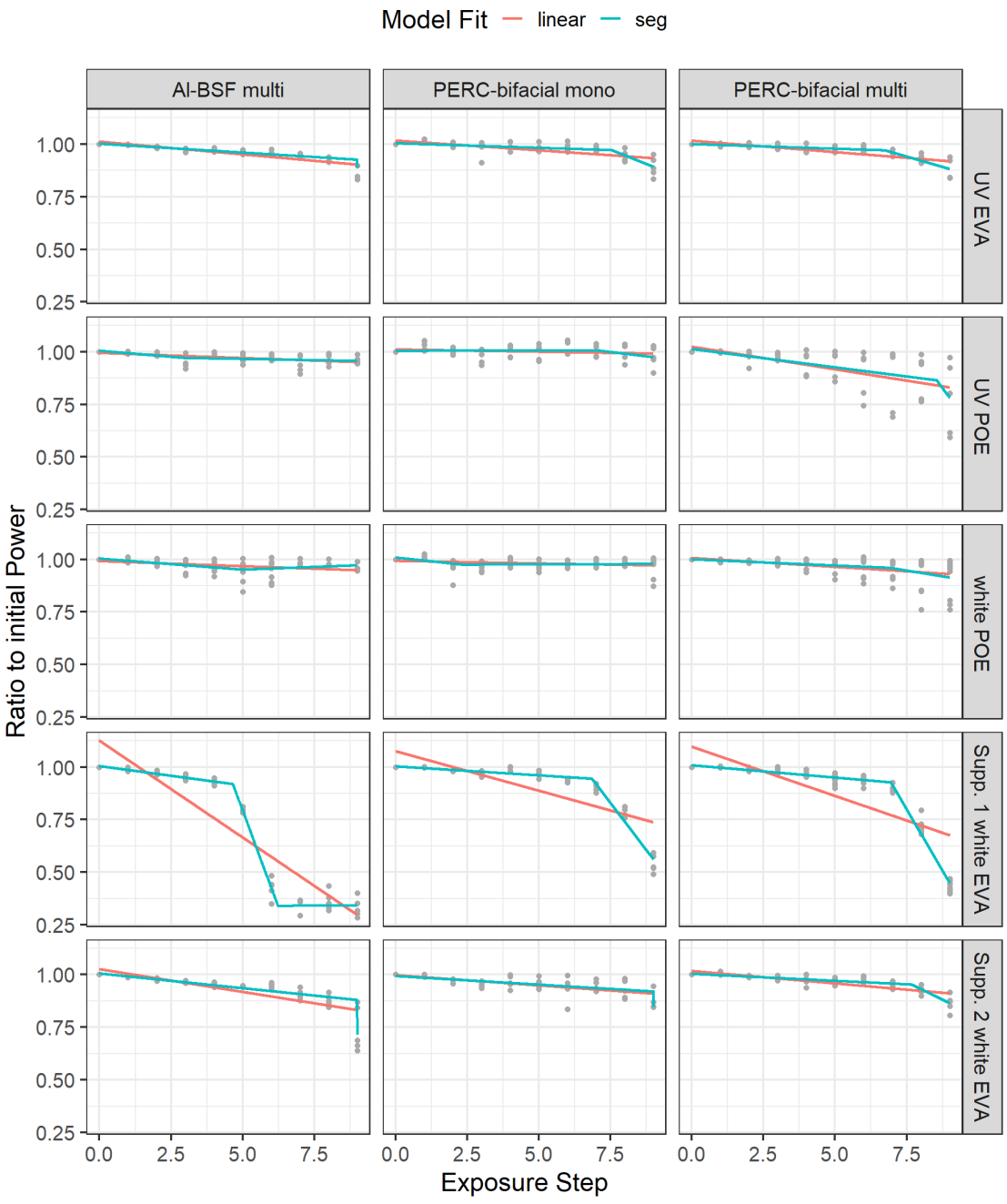

Figure 4: Stepwise P_{mp} measurements divided by the initial power of each sample for the mDH+FS exposure. Data are divided by packaging and cell combinations with linear and piecewise linear models being shown for each.

assess any variations between them. As TiO_2 is known to produce free radicals through photo-excitation, the quality of the TiO_2 may have a strong influence on the stability of the EVA and subsequently the module as a whole.

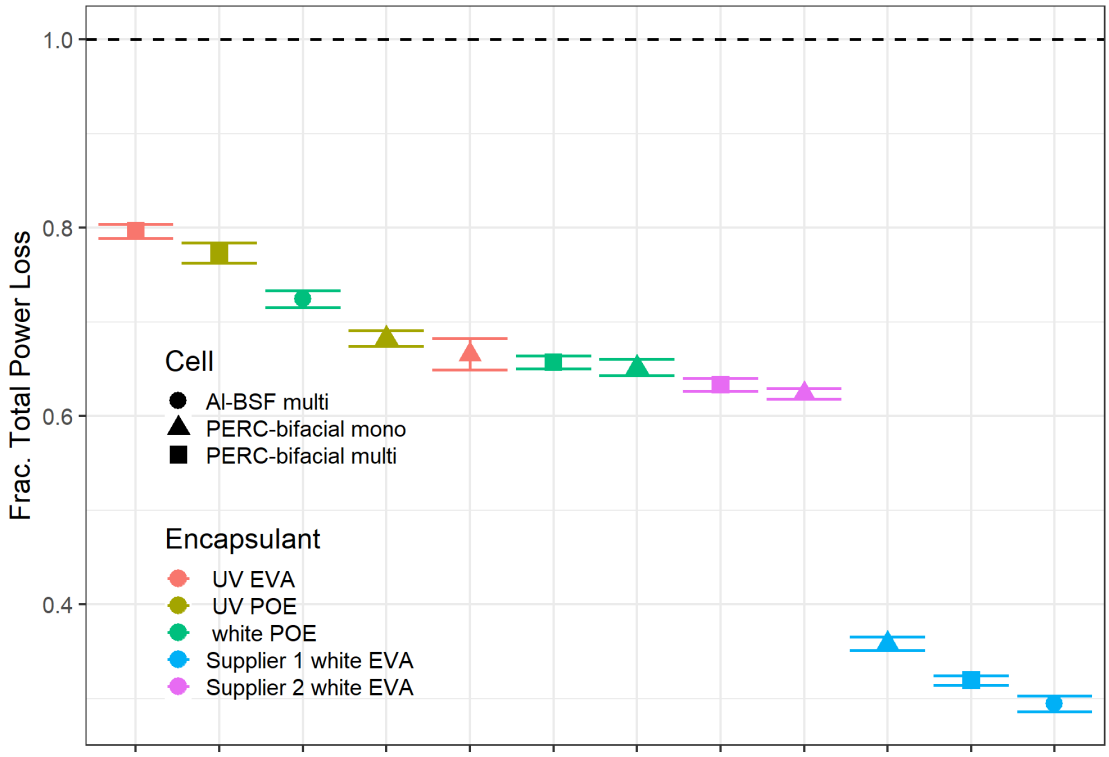

Figure 5: Fraction of final P_{mp} compared to initial for the piecewise linear models of the mDH samples. Error bars shown are 83.4% confidence intervals.

3.2 University of Central Florida

UCFs primary focus has been the sectioning of modules and minimodules and the analysis there of, in partnership with UConn.

Materials Characterization on Full Sized Modules

Previously we cored out samples from the full-sized modules and performed top-down SEM, EDS and XPS analysis. To gain some more confidence in our analysis, we further performed XPS imaging alongside XPS spectrum. XPS imaging allows us to visualize the location of the detected elements. A Thermo Scientific ESCALAB-250Xi spectrometer with an ultra-high vacuum (UHV) chamber (below $7 \cdot 10^{-9}$ mbar) was used for the analysis. XPS imaging was recorded with the full range of the spectrum after 20 level of depth profiling. 650 μm spot size with lower pass energy (20 eV) was utilized for better resolution imaging. Our results from EDS and previous XPS suggested that the Ag gridlines were oxidizing and there is presence of Sn alongside Pb. Sn was not originally present in the Ag paste. However, the solder used for the interconnects is Pb-Sn solder. Therefore, Sn might have migrated from the interconnects to the gridlines. The XPS imaging (Fig. 7) confirms the presence of Pb and Sn alongside Ag on the gridlines of degraded samples. We confirmed that there is no Sn in the control samples. We believe that this skin layer of SnO_2 is contributing to the acceleration of the metal-Si interfacial corrosion that is degradation the contacts resulting in high resistance and dark areas seen in EL imaging.

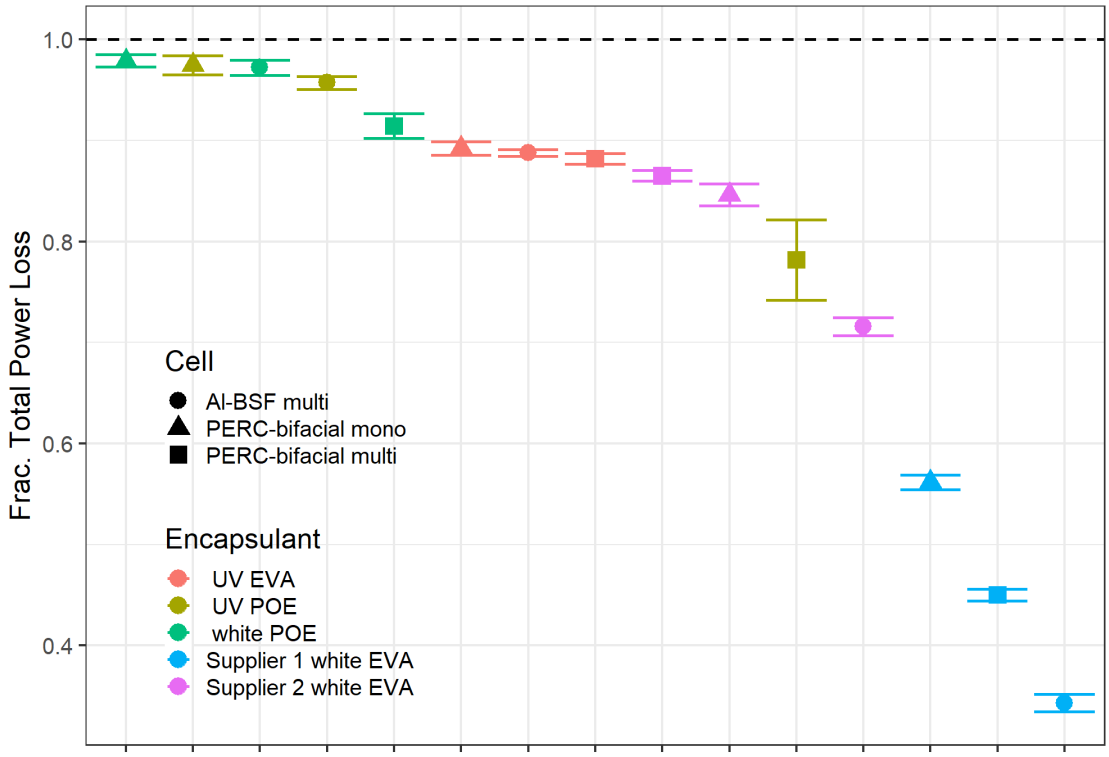

Figure 6: Fraction of final P_{mp} compared to initial for the piecewise linear models of the mDH+FS samples. Error bars shown are 83.4% confidence intervals.

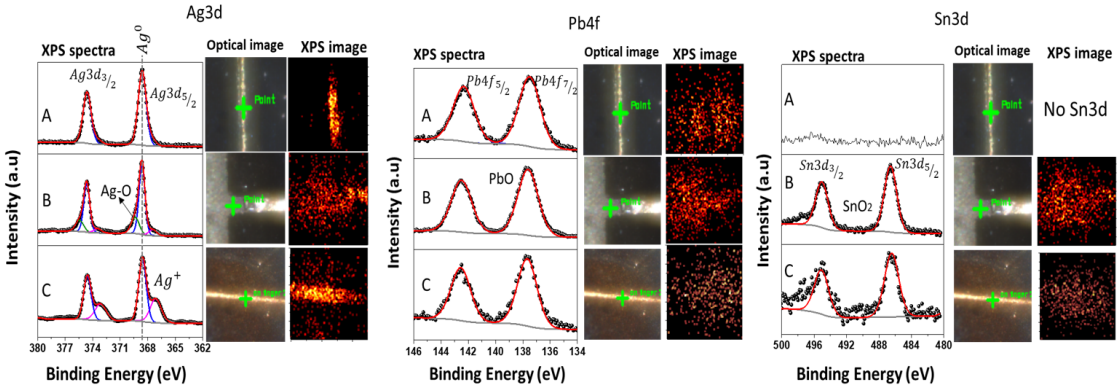

Figure 7: XPS elemental comparisons between cored samples from different modules
A: Control monocrystalline PERC module
B: Degraded monocrystalline PERC
C: Degraded multicrystalline Al-BSF.

mDH Mini Modules Dark vs. Illuminated R_S

Dark R_S is calculated using a simple linear regression for values in the range of $0.01I_{SC} - 1I_{SC}$. A range of $0.01I_{SC} - 1I_{SC}$ was also explored (Fig. 8). Illuminated RS is calculated using the I-V data with pseudo-I-V generated using Suns-VOC. The two values are compared for each

module with the exception of sa42800 because it had a faulty junction box. While the first range of current values extends far below that of the dark I-V curve's linear regime, it gives dark R_S values most closely approximating illuminated R_S. The R^2 values also improved from 0.843 to 0.887 when increasing the range of current values. Underestimation in R_S has been seen before for cells. We have previously seen that for full-sized modules undergoing contact corrosion, such as that observed in the mDH mini modules, dark measurements tend to underestimate the R_S.

This could be because out of the total corroded contact area, corrosion in the lateral contacts (fingers) takes up the majority when compared to busbar/interconnection corrosion. This would influence the resistance in illuminated measurements more than in dark measurements because photo-generated carriers distributed across the active cell surface area are more greatly impeded than injected carriers through the interconnections. Carriers injected in the dark have a more direct path to travel - interconnect to busbar to area directly beneath contact to rear metallization. While there is lateral transport in dark injection, the impact of gridline corrosion is not as significant to impeding carrier motion as when the carriers are distributed across the entire active cell surface area.

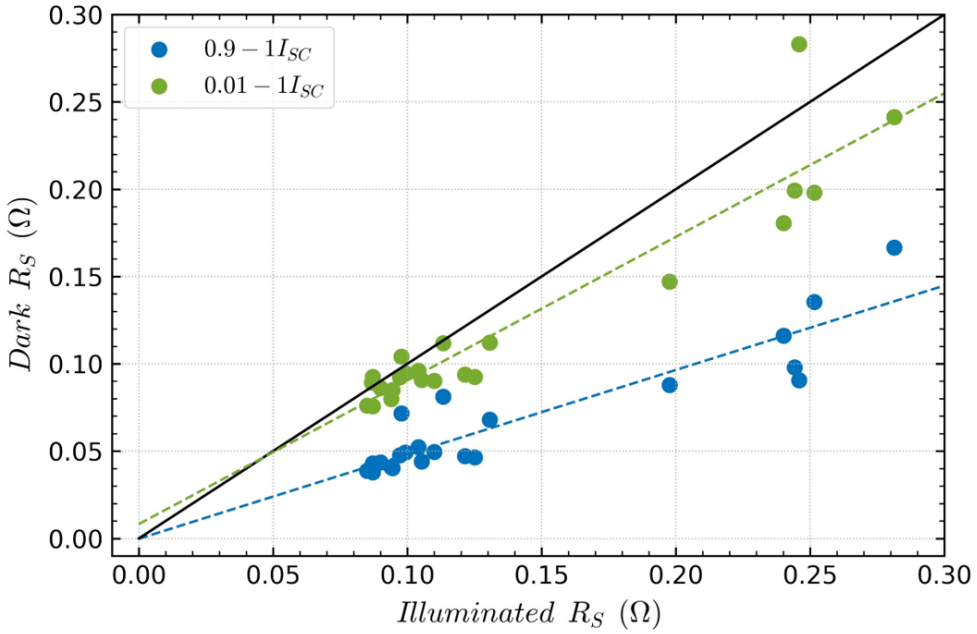

Figure 8: Illuminated vs. dark I-V for multiple current ranges.

Materials Characterization on Cored Samples from mDH Mini Modules

Samples from the degraded regions were cored out from mDH mini modules for materials characterization. Top-down SEM imaging was performed to look for visual signs of degradation. SEM images in Fig. 9 show signs of delamination, degradation and imprints for both the mono-PERC and multi-PERC samples.

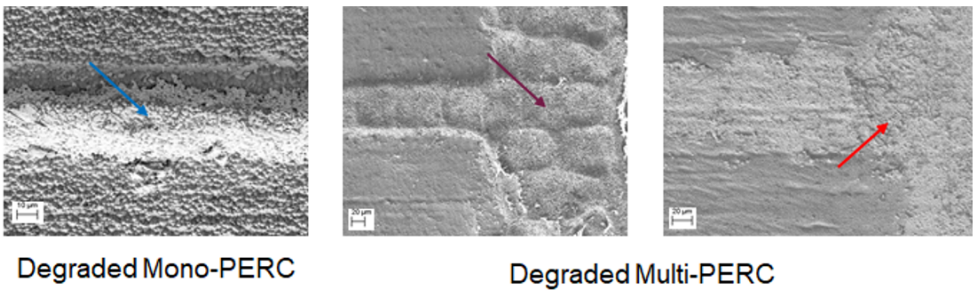

Figure 9: SEM imaging of degraded minimodule busbars and gridlines for multiple samples.

XPS analysis was also performed on these samples and compared with the control sample, shown in Fig. 10. XPS spectra shows oxidation of Ag and presence of Pb. Interestingly, no Sn was observed on the degraded sample. Further investigation is being performed to understand the degradation mechanism for this group of samples.

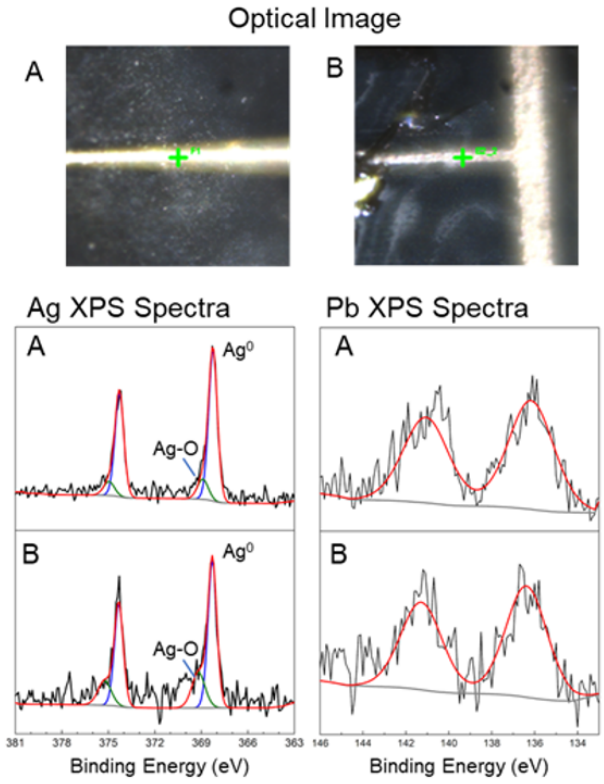

Figure 10: XPS results from minimodule cored samples
A: control
B: degraded multi-PERC.

PVSC 2021 Submission

Multiscale Characterization to Study Contact and Interconnect Degradation in Solar Cells

Nafis Iqbal[1,2], Dylan J. Colvin[1,2,3], Alan J. Curran[4], Jean-Nicolas Jaubert[6], Fang Li[6], GovindaSamy TamizhMani[6], Roger H. French[4] and Kristopher O. Davis[1,2,3,7]

[1]Department of Materials Science and Engineering, University of Central Florida, Orlando, Florida, USA
[2]Resilient Intelligent Sustainable Energy Systems Faculty Cluster, University of Central Florida, Orlando, Florida, USA
[3]FSEC Energy Research Center, Cocoa, Florida, USA
[4]Materials Science and Engineering, Case Western Reserve University, Cleveland, Ohio, USA
[5]Canadian Solar, Inc., Guelph, Ontario, Canada
[6]Photovoltaic Reliability Laboratory, Arizona State University, Mesa, USA
[7]CREOL, the College of Optics and Photonics, University of Central Florida, Orlando, Florida, USA

***Abstract*—The current popularity of photovoltaic (PV) systems is due to the fact that they are exceptionally reliable and significantly lower cost than other energy sources. Studying module degradation is key to promote further development in the state of the art. Fielded or accelerated aged modules exhibit different failure modes, of which metallization degradation (contacts and interconnections) is prevalent. In this work, we apply multiscale characterization to a variety of module technologies that have been field exposed and have undergone accelerated age testing. The observed performance losses are then related to materials properties to find out the root cause of degradation. The initial characterizations include module and cell-level current-voltage (*I-V*), Suns-V_{OC}, photoluminescence (PL) and electroluminescence (EL) imaging. Samples are then extracted from particularly degraded regions of the module and prepared for top-down and cross-sectional scanning electron microscopy (SEM), energy dispersive spectroscopy (EDS) and X-ray photoelectron spectroscopy (XPS), allowing a deeper look into the chemistry behind the metallization degradation. Here we summarize our work on the application of multiscale characterization methods to study contact and interconnect degradation in different module types. We show some of our findings for each characterization steps and how they can be related to determine the specific failure mechanisms.**

***Index Terms*—multiscale characterization, metal contacts, interconnects, contact degradation, reliability**

I. Introduction

The impressive reliability and durability (low power degradation) has made photovoltaic (PV) modules highly competitive with other energy sources [1]. The innovations that made PV modules durable came from studying degradation. Contact and interconnection degradation has been shown to be prevalent in the field [2]–[5]. Examples include grid interruptions, contact voids, contact corrosion, high resistance/recombination, snail-trail, and interconnect breakage [6]–[8]. A more statistical approach to study these degradation is to perform multiscale characterizations on a large and diverse population of modules. Multiscale characterization methods can be used to link observed degradation to specific loss mechanisms (*i.e.*, optical, recombination, resistive) and to the root causes (*i.e.*, changes in chemistry and/or microstructure). Our analyses start with analyzing full-sized modules and then working down to nanometer-scale films and interfaces as needed. The benefit of this characterization sequence is that changes in module performance can be associated with changes in material properties, thus giving a more fundamental understanding of degradation mechanisms and point more closely toward potential solutions. Each of the characterization techniques can be applied in a few different ways as necessary for any specific module. Also, the large data-set generated during these experiments improves the level of confidence in analyzing the data and determining the failure mode. In this work, a summary of our multiscale characterization sequence is discussed with examples from various different experiments. We also discuss some of our findings for different modules and how all the data is linked to determine the failure mechanisms.

II. Experiment

A. Module and Cell Characterization

First the selected modules are inspected for visual signs of degradation. The modules are then inspected in detail via a series of characterizations like module and cell level current-voltage (*I-V*), Suns-V_{OC}, photoluminescence (PL) and electroluminescence (EL) imaging. The data from these characterizations help determine modules that need further investigation. Samples are then extracted from the degraded regions of the modules followed by the removal of encapsulant and backsheet to prepare for materials characterization.

B. Materials Characterization

Top-down and cross-sectional scanning electron microscopy (SEM), energy dispersive spectroscopy (EDS) and X-ray photoelectron spectroscopy (XPS) analysis on the metal contacts and interconnects are performed to understand the mechanism behind degradation.

III. Results and Discussion

The initial characterization suite (I-V, EL, PL, Suns-V_{OC}) helps in analyzing the performance losses of the modules. They also allow in locating regions of module with significant contact and interconnect degradation. Fig. 1 shows EL images of a monocrystalline and a multicrystalline module that went through multiple steps of damp-heat exposure. The multicrystalline module shows darkening all over the cell, but the monocrystalline module shows a unique darkening pattern starting from the busbar. The most likely mechanism for this unique pattern is the degradation of contacts. Therefore, samples are cored out from the dark regions for further analysis.

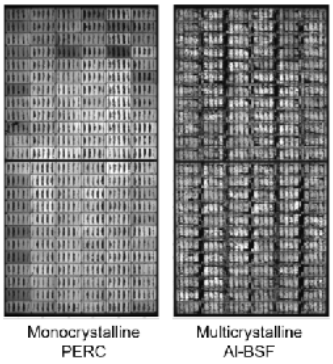

Fig. 1. EL images of monocrystalline and multicrystalline modules after multiple steps of damp heat exposure.

I-V and Suns-V_{OC} measurements are performed at each step of this experiment which help to determine how the performance is impacted. Fig. 2 shows the results from I V measurement taken at each step of DH exposure. It is clear from the trend that the multicrystalline module degrades more than the monocrystalline. Also, it is clear that the performance losses seen are mainly related to resistive issues which can be linked to degradation of contacts and interconnects.

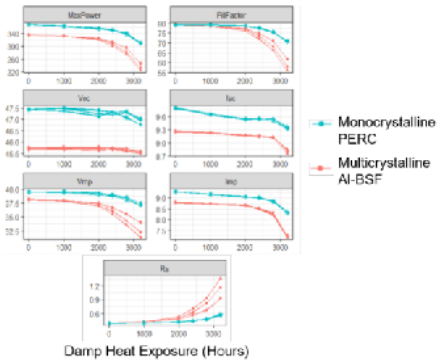

Fig. 2. Multi-step I-V recorded at each step of damp-heat exposure.

After locating the degraded areas in a module, samples are cored out for materials characterization. Fig. 3 shows an image of our coring process and the final sample after removal of EVA. Our coring process is similar to "partial coring" used in [9]. A drill press equipped with a mill bit of 0.5 inches in diameter is used for coring. This process is carefully carried out to extract samples without inducing any damage (such as cracks) or chemistry changes (due to heat).

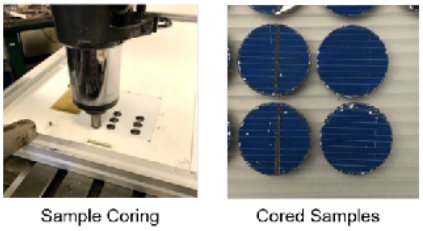

Fig. 3. Sample coring and final samples prepared for materials characterization.

Similar characterizations are also performed on modules exposed in the field. Fig. 4 shows experiment done on modules that were exposed in Florida and Arizona climates for 10 and 18 years respectively [10]. Their performance were compared with an unexposed control module. Strips were extracted to perform contact resistivity measurement using the transmission line method (TLM) [11]. The results suggest that the contacts for the Arizona samples degrade more than Florida samples.

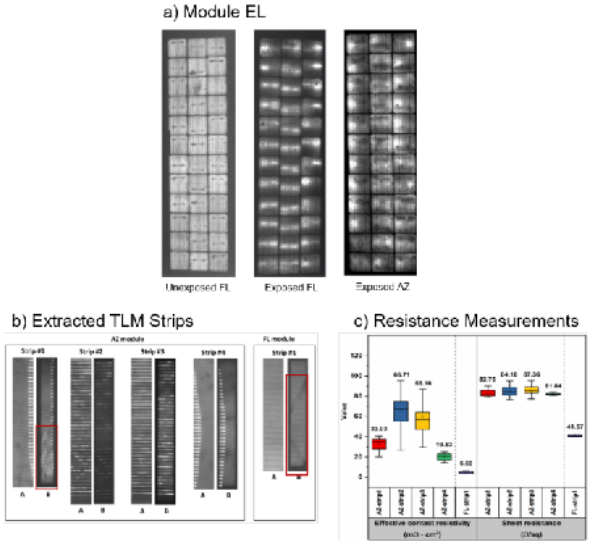

Fig. 4. (a) EL images for modules exposed in Florida and Arizona climate (b) TLM stips extracted from modules (c) Resistance measurements performed on extracted samples.

The samples extracted from the degraded regions of a module are analyzed with different materials characterization techniques. Top-down SEM and EDS is performed to check

for visual signs of degradation. It also allows to see if there is migration of unwanted elements onto the surface of contacts and interconnects with possible change in surface chemistry. Fig. 5(a) shows top-down SEM & EDS performed on top of a degraded contact for a sample cored out from monocrystalline module shown in Fig. 1. The SEM image clearly shows signs of delamination on a finger that is near the busbar. EDS reveals the presence of Sn on the fingers along with Ag. Cross-sectional SEM is also performed to check for degradation in the interfaces. Fig. 5(b) shows cross-sections of good and degraded contacts. The degraded contact shows particles embedded in the interface which means there is formation of gap in the metal-silicon interface of the contact. This can lead to higher series resistance seen in Fig. 2.

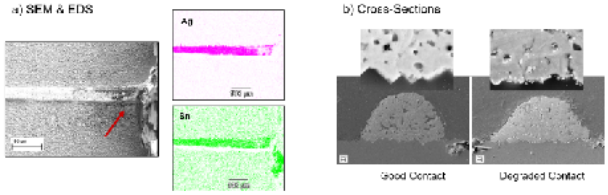

Fig. 5. Examples of (a) top-down SEM & EDS (b) cross-sectional SEM.

XPS analysis is performed to get detailed insights into the materials properties. Depth profile is performed to see the change from surface towards the interface. Fig. 6(a) shows XPS performed on the cored samples from accelerated aged modules shown in Fig. 1. It is noticeable how the chemistry of the Ag is different, strongly suggesting that the degradation is related to paste composition of the metal contacts. The DH stability is therefore related to the paste composition used for different technologies. Fig. 6(c) and (d) show similar studies performed on field exposed modules shown in Fig. 4. Here the focus is on the C and O spectrum to learn the effect of encapsulant in the contact and interconnect degradation.

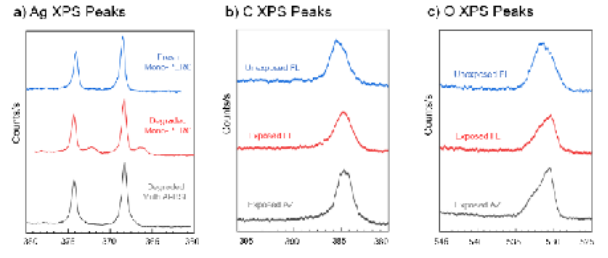

Fig. 6. (a) Ag XPS analysis performed on cored samples that went through damp-heat exposure. C and O XPS analysis performed on field exposed modules (b) and (c).

IV. Conclusion

Multiscale characterization methods can be a powerful tool to study contact and interconnect degradation. The large datasets collected from this study can help boost confidence in the observations made and the interpretation of the analyses. It will also help to gain deeper insight into the observed failure modes and determine the root causes. In this work, we summarize our approach to apply multiscale characterization methods to PV modules. This method has the flexibility to be applied widely to any module technology. We show our results obtained by applying this method and our investigation of the root cause of failure.

Acknowledgment

This material is based upon work supported by the U.S. Department of Energy's Office of Energy Efficiency and Renewable Energy (EERE) under the Solar Energy Technologies Office Agreement Number DE-EE0008172 and DE-EE0008155.

References

[1] D. C. Jordan, B. Marion, C. Deline, T. Barnes, and M. Bolinger, "Pv field reliability status—analysis of 100 000 solar systems," *Progress in Photovoltaics: Research and Applications*, 2020.

[2] M. Köntges, G. Oreski, U. Jahn, M. Herz, P. Hacke, and K.-A. Weiß, *Assessment of photovoltaic module failures in the field: International Energy Agency Photovoltaic Power Systems Programme: IEA PVPS Task 13, Subtask 3: report IEA-PVPS T13-09:2017*. Paris: International Energy Agency, 2017.

[3] S. Yang and T. Jiang, "Crystalline Silicon PV Module Field Failures," in *Durability and Reliability of Polymers and Other Materials in Photovoltaic Modules*. Elsevier, 2019, pp. 171–216. [Online]. Available: https://linkinghub.elsevier.com/retrieve/pii/B9780128115459000082

[4] R. Dubey, S. Chattopadhyay, V. Kuthanazhi, A. Kottantharayil, C. Singh Solanki, B. M. Arora, K. L. Narasimhan, J. Vasi, B. Bora, Y. K. Singh, and O. S. Sastry, "Comprehensive study of performance degradation of field mounted photovoltaic modules in India," *Energy Science & Engineering*, vol. 5, no. 1, pp. 51–64, Feb. 2017. [Online]. Available: http://doi.wiley.com/10.1002/ese3.150

[5] K. Kato, "PV module failures observed in the field," p. 18.

[6] A. Kraft, L. Labusch, T. Esslen, I. Dürr, J. Bartsch, M. Glatthaar, S. Glunz, and H. Reinecke, "Investigation of acetic acid corrosion impact on printed solar cell contacts," *IEEE Journal of Photovoltaics*, vol. 5, no. 3, pp. 736–743, 2015.

[7] E. J. Schneller, R. P. Brooker, N. S. Shiradkar, M. P. Rodgers, N. G. Dhere, K. O. Davis, H. P. Seigneur, N. Mohajeri, J. Wohlgemuth, G. Scardera *et al.*, "Manufacturing metrology for c-si module reliability and durability part iii: Module manufacturing," *Renewable and Sustainable Energy Reviews*, vol. 59, pp. 992–1016, 2016.

[8] G. Wilson, M. M. Al Jassim, W. Metzger, S. W. Glunz, P. Verlinden, X. Gang, L. Mansfield, B. J. Stanbery, K. Zhu, Y. Yan *et al.*, "The 2020 photovoltaic technologies roadmap," *Journal of Physics D: Applied Physics*, 2020.

[9] H. Moutinho, B. To, D. B. Sulas-Kern, C.-S. Jiang, M. Al-Jassim, and S. Johnston, "Advances in Coring Procedures of Silicon Photovoltaic Modules," in *2019 IEEE 46th Photovoltaic Specialists Conference (PVSC)*. Chicago, IL, USA: IEEE, Jun. 2019, pp. 2008–2012.

[10] A. Sinha, F. Li, V. S. P. Buddha, E. J. Schneller, K. O. Davis, and G. TamizhMani, "Contact resistivity and sheet resistance measurements of cells extracted from field-aged modules," in *2019 IEEE 46th Photovoltaic Specialists Conference (PVSC)*. IEEE, 2019, pp. 2003–2007.

[11] S. Guo, G. Gregory, A. M. Gabor, W. V. Schoenfeld, and K. O. Davis, "Detailed investigation of tlm contact resistance measurements on crystalline silicon solar cells," *Solar Energy*, vol. 151, pp. 163–172, 2017.

3.3 University of Connecticut

FIB and SEM cross-sectioning continued in order to image the microstructure and composition beneath top surface electrode fingers for monocrystalline PERC specimens that underwent accelerated degradation in comparison with un-degraded sister samples. A degraded BSF is also queued up for FIB sectioning and SEM analysis, but planned holiday shutdowns as well as unplanned facility issues delayed this additional information. Each of these 3 primary specimens was previously examined at the macroscale. Results below are focused on the undegraded PERC sample, and comparisons with the previously reported similar measurements for the degraded sample. Fig. 11 displays oblique-perspective SEM images of the un-degraded PERC sample in the vicinity of a top electrode finger, pre- and post- FIB. A montage of higher magnification secondary electron images reveals moderate 'curtaining' from the ion milling process, i.e. roughly parallel vertical lines that result from the ion beam directed from top to bottom for this field of view. Aside from this subtle artifact, however, the images resolve the pyramidal front surface facets, the polycrystalline nature of the electrode finger, substantial twinning within individual grains of the finger distinguishable by their differing orientation as well as subtle contrast variations resulting from electron channeling effects, and finally numerous electrode pores with sizes ranging from 50nm to 1µm. EDS spectra acquired at several locations identify Si, Ag, C, Pb, and Na among the composition notably along the interface with the Si cell.

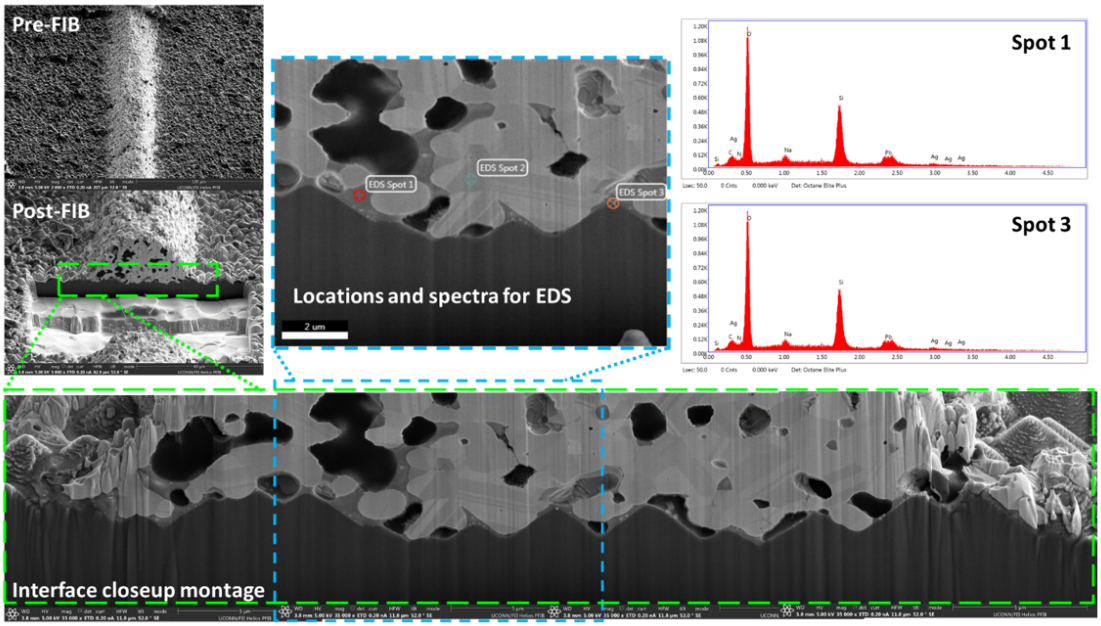

Figure 11: Oblique SEM (secondary electron) image of a front surface electrode finger for an un-degraded PERC cell before and after site-selective FIB cross-sectioning; magnified montage of images along the interface; and regions of interest along with compositional analysis via EDS spectra at distinct interface positions.

Compositional mapping in this same vicinity, Fig. 12, confirms a relatively uniform concentration of these various chemical elements within the electrode finger (aside from the pores which are uniformly dark). Oxygen is the most obvious exception, indicative of the glass frit that en-

hances the annealing process. Albeit barely distinguishable in the EDS spectra, Nitrogen is also visible in the EDS maps, specifically along the interface corresponding to the front surface nitride passivation layer. Although this nitride therefore still remains in some locations, it is evidently discontinuous after the electrode annealing step in order to negligibly affect conduction through the interface.

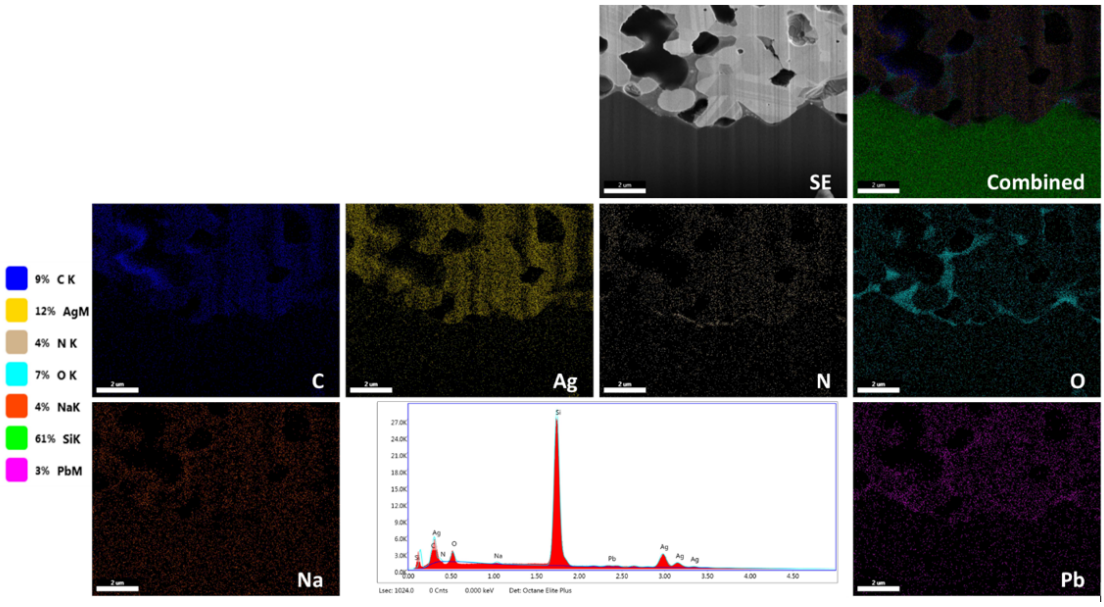

Figure 12: EDS composition mapping identifying relative concentrations of several elemental species as labelled (same general region as prior figure) for a PERC cell following accelerated aging.

For comparison, Fig. 13 shows an equivalent analysis at the front PERC-electrode finger interface for a degraded cell. Microstructurally and compositionally these specimens are similar. Other work suggested that a likely species associated with degradation may be Sn, possibly redeposited from solution during humidity-enhanced corrosion especially at the finger/Si interface, but Sn was not observed in either the aged specimen or the control. Additional sectioning of the aged specimen is underway, especially closer to the bus-bars which would be the source of the Sn via a different solder composition for these larger electrode structures as compared to the fine, ink-jet printed, primarily silver silicide fingers.

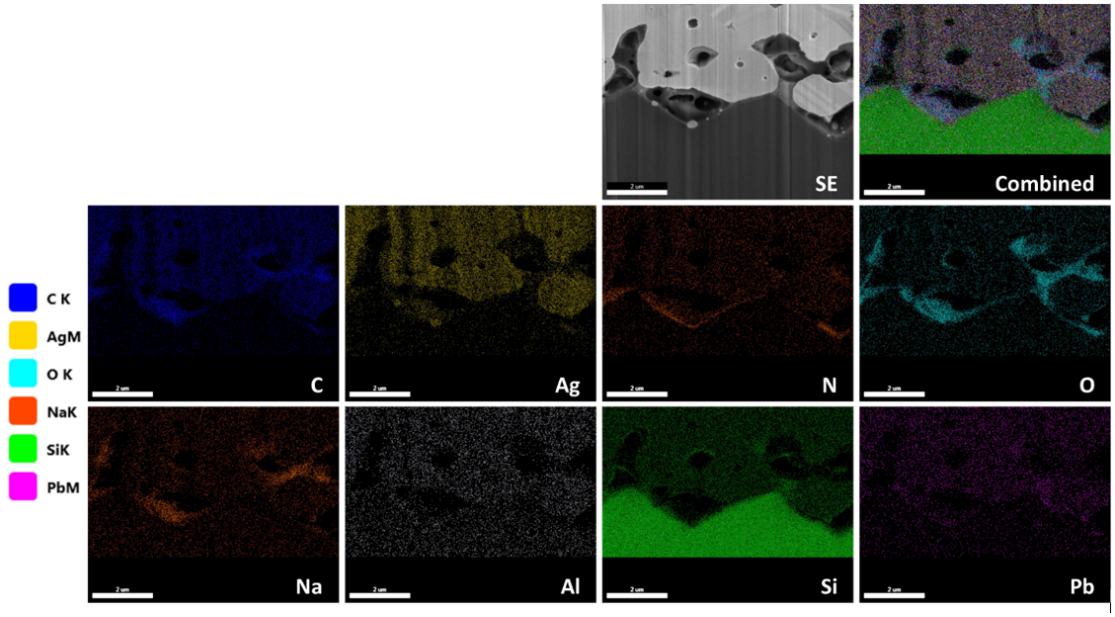

Figure 13: EDS composition mapping for an as provided (non-aged) PERC cell for comparison.

Separately, we are contributing content to the cumulative review of degradation in crystalline silicon cells. In particular, we are focusing on tandem cells comprising hybrid perovskites mated to a conventional Si cell. Given their wide bandgap, absorption tunability, and an appropriately cautious industry when it comes to introducing new materials or designs, tandem devices comprising a hybrid perovskite solar cell on top of a silicon cell are certain to be the route by which HP's begin to make substantial inroads into the worldwide solar energy production. Indeed, tandem cells already achieved a certified PCE of 29.15%,[3] generally assembled as in Fig. 14 with a hole transport layer, thin film halide perovskite (b, typically CH3NH3PbI3), electron transport layer, and transparent conducting oxide atop a PERC or similar silicon cell.[4] However, the HP layer is typically polycrystalline (c), highly susceptible to humidity, and also sensitive to heat and light induced degradation. Furthermore, many complex designs and manufacturing advances are still being explored to optimize efficiency, reliability, and marketability, including substituting environmentally less concerning ions for Pb, replacing the MA cation and I anions with potentially more stable species, grain size control, grain boundary doping or passivation, layered structures or finer composition gradients, incorporating 2-d materials, and even leveraging the possibility of ferroelectricity and its concomitant built-in fields to enhance carrier separation. This creates numerous challenges for reliability that will need to be addressed before such crystalline silicon and hybrid perovskite tandem cells become truly competitive with the 30 year performance of current generation panels (PERC) and prior technologies (BSF, etc.), especially under real-world operating conditions.

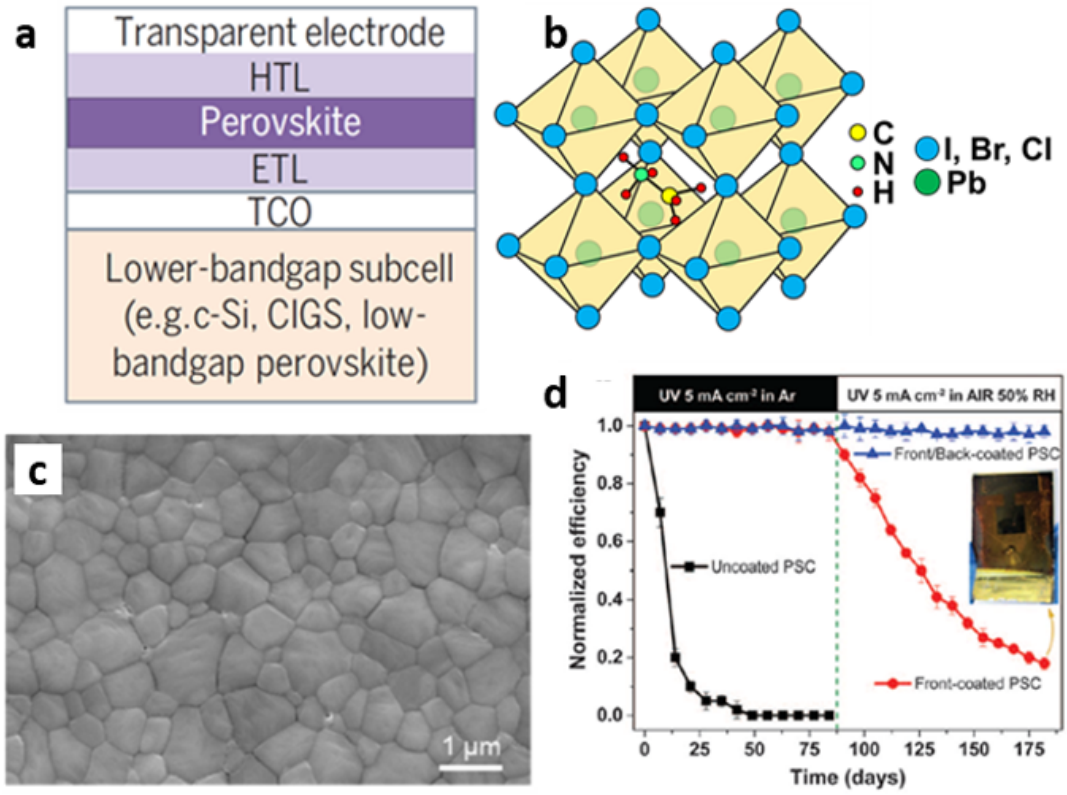

Figure 14: Representative tandem crystalline silicon and hybrid perovskite solar cell stack (a), unit cell for typical methyl ammonium lead triiodide (MAPbI3) HP layer (b), polycrystalline nature even of high performance HP films (c), and one early example of degradation studies for perovskite solar cells (d). Note Fig. 14 a-b adapted from [3], c adapted from [5], d reproduced from [6].

3.4 Canadian Solar

Canadian Solar has progressed the passivation sample exposure to completion. They have shipped the samples from said study to our partners at UCF for further sample coring and characterization.

As we start to move more strongly into monofacial and bifacial PERC as industry staples, we want to focus more specifically on what we might refer to as PERC specific degradation mechanisms. The passivation layer is the component that defines a PERC cell, and its stability is an important area of study. So far in our exposures, we have not been able to directly test or measure the passivation region, although we are moving towards that with our sample coring at UCF and UConn. To this extent, we have started an exposure specifically to target the UV stability of these passivation regions.

To investigate PERC UV degradation, PERC cells with 3 types of passivation designs are made into one-cell mini-modules and being aged under a full-spectrum metal halide UV lamp with UV irradiance of $150W/m^2$. Either the front side or rear side of one PERC type is exposed to UV, while the other two types are exposed only on the front side. Details of the passivation and cell types are given in Figs. 15 and 17, while the metrics of the tests run on the samples is given in Figure 16. Before UV, the preconditioning procedures were carried out to get rid of LID, including $10kWh/m^2$ of sunlight simulator and then subsequently 48 hours of I_{SC} at $80C^o$.

Group	Wafer	Cell type	Busbar	Front passivation	Rear passivation
1	Multi-p	Bi-PERC	9BB	SiNx(plate PECVD)	Al2O3(plate ALD)/SiNx(tube PECVD)
2	Multi-p	Bi-PERC	9BB	SiNx(tube PECVD)	Al2O3(plate ALD)/SiNx(tube PECVD)
3	Multi-p	Bi-PERC	9BB	SiNOx/SiNx/SiOx	Al2O3(plate ALD)/SiNx(tube PECVD)
4	Multi-p	Bi-PERC	9BB	SiNx(plate PECVD)	Al2O3(plate ALD)/SiNx(tube PECVD)

Figure 15: Sample passivation variation of the CSI UV study.

Passivation	No.	Preconditioning	Tests	Stresses	UV exposure and tests Step: 7 days or ~21 kWh/m^2
Group 1	G1-1 (Baseline)	Light 10kWh/m2 + CID 48h	SunVoc PL EL EQE	Room temp Without light	\
	G1-2 (No UV)			60 ℃ No UV (covered)	Initial, Preconditioning, 7d, 14d, 21d, 28d, 35d, 42d Each step: SunVoc EL PL EQE
	G1-3			60 ℃ UV 125 W/m^2	
	G1-4				
	G1-5				
	G1-6				
Group2	G2-1				

Figure 16: Exposure layout for the UV passivation samples. Each sample type will have 6 total mini-modules undergoing various exposure.

Items	G1	G2	G3	G4
	Front	Front	Front	Rear
Texturing	Random pyramids	Random pyramids	Random pyramids	Random pyramids
Emitter Sheet Resistance	145	145	135	145
Anti-PID equipment	Ozone	Ozone	Thermal-Oxidation	Ozone
Etching type	Acid	Acid	Acid	Acid
PE type	Plate PECVD	Tube PECVD	Tube PECVD	Tube PECVD
Thickness	82nm	82nm	85nm	90nm
Refractive Index	2.08	2.08	2.05	2.1
Layer Structure	SiNx	SiNx	SiO2+SiNx+SiNOx	SiNx
				15nm Al2O3 (Plate ALD)

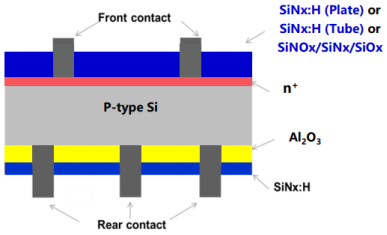

Figure 17: Detailed information about the passivation construction.

The results of the exposure have been drafted into a submission for PVSC. The abstract is shown below.

PVSC 2021 Submission

Impact of surface passivation on UV stability of bifacial mc-Si PERC solar modules

Ben X. J. Yu[1], Jean-Nicolas Jaubert[1], Guangchun Zhanng[1], Dylan Colvin[2,3], Nafis Iqbal[2,3], Kristopher Davis[2,3], Thomas Moran[4], Bryan Huey[4], Alan Curran[5], Laura Bruckman[5], Jennifer Braid[5], Roger French[5]

[1]*CSI Reliability Research, Canadian Solar Inc.*, Suzhou, Jiangsu, China
[2]*Materials Science*, *University of Central Florida*, Orlando, FL, USA
[3]*FSEC Energy Research Center*, Orlando, FL, USA
[4]*Materials Science*, *University of Connecticut*, Storrs, CT, USA
[5]*Materials Science*, *Case Western Reserve University*, Cleveland, OH, USA

***Abstract*—Many research shows that UV degrades the solar cell and module power. In this work, we study the UV stability of mc-Si bifacial PERC solar modules with different industrial silicon nitride (SiNx) passivation. We find that with exposure to UV at 60 °C, both V_{OC} and J_{SC} decrease then stabilize. The quantum efficiency analysis shows decreased response in both short (blue loss) and long (base collection loss) wavelength range. It infers that deteriorations were not only at passivation layers, but also in the silicon bulk, caused by UV-induced degradation and possible LeTID. No significant difference in degradation has been found between front and rear passivation, or between different form factors of PECVD devices, respectively. The passivation of SiNOx/SiNx/SiOx using thermal oxidation processing shows the best resistance to UV.**

Keywords—PERC, Multicrystalline, Bi-Facial, UV-induced degradation, Passivation, PECVD, Thermal oxidation

I. Introduction

Encapsulation with high UV transmission has been used by solar panel manufacturers to harness spectral response of solar cells in the shorter wavelength range. However, Sinha et al. reported induced UV exposure caused equivalent power loss ranging from commonly seen 0.5%/y up to 8%/y for raw solar cells with various technologies after exposure to UV irradiation of 8.92 $MJ/m^{-2}{\cdot}nm^{-1}$ at 340 nm [1]. Witteck et al. concluded that UV photons broke Si-H bond and increased the recombination at the passivation surface [2,3]. While Ye et al. found that UV light triggered the generation of defect in the bulk of solar cells [4].

Since passivated emitter rear contact (PERC) is currently the most dominant solar cell technology in PV market and is anticipated to be so in next few years [5], this work focuses on degradation of bifacial PERC with common silicon nitride (SiNx) passivation stacks. We study the impact of passivation property on the UV performance of multicrystalline (mc-Si) PERC solar cells and aim to find the best strategies to mitigate UV-induced degradation.

II. Experiment

A. Sample preparation

Boron-doped mc-Si PERC cells were fabricated in an industrial PERC production line. A layer of Al_2O_3 were deposited on the rear surface of cell via atomic layer deposition (ALD). The front and rear surfaces were then further coated with different designs of SiNx:H by either plate or tube plasma–enhanced chemical vapor deposition (PECVD) as shown in Figure 1. In particular, SiOx were introduced by thermal oxidation.

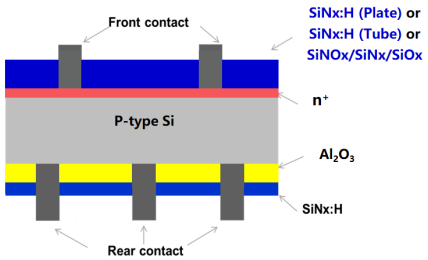

Fig. 1. Scheme of fabricated bifacial PERC cells with different front passivation.

Four groups of one-cell minimodules composed of the same glass, encapsulant, and backsheet were prepared using fabricated PERC cells. The groups of minimodules differ on the basis of passivation surface irradiated by UV, as shown in Table 1 and Figure 2. G1, G2, G3 are regular modules with cell front passivation on the glass side, while G4 has the same PERC cell as G1 but with cell rear passivation on the glass side. The UV light source was metal halide lamp with visible lights not being filtered.

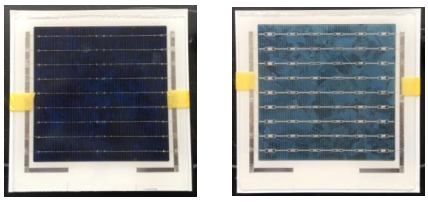

Fig. 2. Images of a G1 minimodule and a G4 minimodule, with cell front on glass side and cell rear on glass side, respectively.

TABLE I. PASSIVATION STACKS, SHADED AREA INDICATING SURFACE EXPOSED TO UV IRRADIANCE

Group	Irradiated Surface	Passivation	
		Front	Rear
G1	Cell front	SiNx (**Plate**)	Al2O3/SiNx (Tube)
G2	Cell front	SiNx (**Tube**)	Al2O3/SiNx (Tube)
G3	Cell front	**SiNOx**/SiNx/**SiOx**	Al2O3/SiNx (Tube)
G4	Cell rear	SiNx (**Plate**)	Al2O3/SiNx (Tube)

UV transparent EVA was used on the glass side, while UV cut-off EVA was used on the backsheet side to avoid the effect of reflected UV light from white backsheet.

B. *UV aging and characterizations*

To stabilize the test samples, B-O light induced degradation and LeTID preconditioning was performed, the minimodules were exposed to 10 kWh/m^2 of sunlight and then injected with current of Isc at 85°C for 48h. After preconditioning, the minimodules were short-circuited and placed under metal halide lamp with stepwise UV exposure up to a total UV dose of 210 kWh/m^2 at 60°C.

Quantum efficiency (Enlitech), Suns-Voc (Sinton) curves, electroluminescence (EL) and photoluminescence (PL) images of minimodules were obtained each step.

III. RESULTS AND DISCUSSION

A. *Pseudo I-V results*

The short circuit current density (Jsc) was derived by spectral response (SR_{sample}) results from external quantum efficiency (EQE) analysis using Equation 1.

$$Jsc = \int E_{AM1.5}(\lambda) * SR_{sample}(\lambda) * d\lambda \quad (1)$$

Where $E_{AM1.5}$ is power density of solar spectrum AM1.5 and λ is wavelength.

Suns-Voc measured irradiance dependent Voc values and produced series resistance (Rs) free pseudo I-V curves. Then Jsc obtained from EQE were used to adjust current density in the Suns-Voc results and produced actual Rs impacted pseudo I-V curves as shown in Figure 3.

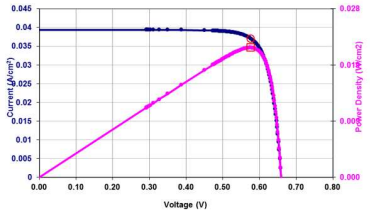

Fig. 3. A typicl SunsVoc pseudo I-V curve.

Finally, I-V features could be extracted from Jsc corrected pseudo I-V curves and the results are shown in Figure 4. G1, G2, and G4 shows similar degradation pattern, with decreased Voc and Isc. While G3 has the least UV-induced degradation.

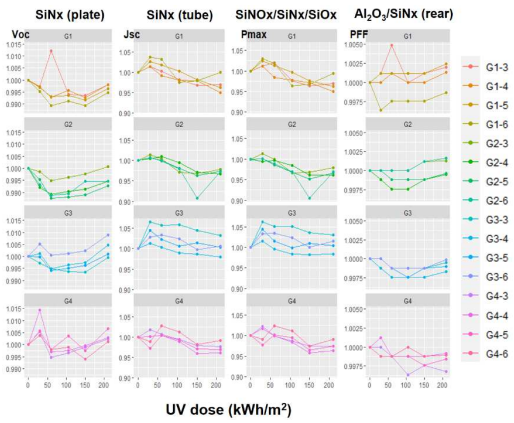

Fig. 4. Jsc corrected pseudo I-V results with exposure of UV.

To obtain good anti-reflection property, the refractive index of SiNx passivation layer for all PERC cells were designed to be 2.1. In order to get the same refractive index, more hydrogen were introduced to SiNx layper prepared by tube PECVD than plate PECVD. The concentration of hydrogen and compactness of SiNx, however, seem not to have a significant impact on UV-induced degradation. By comparing results of G3 with other groups, it can be concluded that thermal oxidation can effectively mitigate the UV-induced degradation.

B. *Spatial response*

Figure 5 shows the average EQE curves of 4 samples of G2 and G4, respectively. Decrease of EQE in the wavelength range

of 400 to 1000 nm has been observed. It can be inferred that deterioration were not only at passivation surface, but also in the silicon bulk.

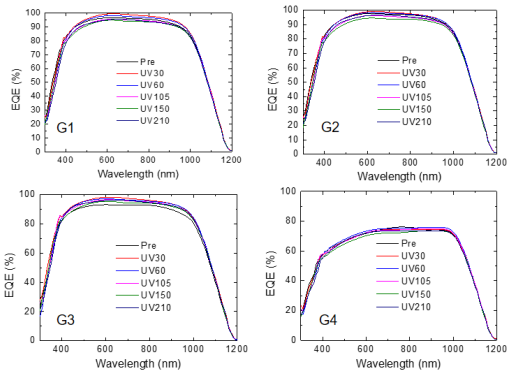

Fig. 5. Mean EQE curves of 4 samples per group.

C. EL, PL

Figure 6 shows typical EL and PL images of module before and after UV exposure. No significant defects can been spotted. Further analysis is required to investigate the mechanism of UV-induced degradation.

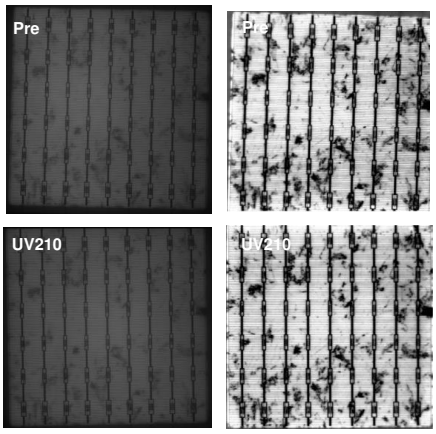

Fig. 6. EL and PL images of G4-2 after preconditioning and UV 210 kWh/m^2.

D. Chemical composition analysis

Composition analysis including coring for element depth profiles, X-ray photoelectron spectroscopy (XPS), Fourier Transform Infrared Spectroscopy (FTIR), and Time-of-Flight Secondary Ion Mass Spectrometry (ToF-SIMS) are on-going for further investigation of degradation mechanism.

IV. Conclusion

We find that thermal oxidation of passivation layer could improve the UV stability of PERC solar module, while similar degradation has been observed between plate and tube PECVD, front and rear passivation, respectively. Results shows that deteriorations were not only at passivation layers and interfaces, but also in the silicon bulk. The degradation most likely were induced by UV photons, however, the impact of LeTID cannot be completely ruled out.

References

[1] Archana Sinha Jiadong Qian Katherine Hurst, et al. "UV-Induced Degradation of High-Efficiency Solar Cells with Different Architectures", 2020 IEEE 47th PVSC, DOI: 10.1109/PVSC45281.2020.9300993.

[2] The International Technology Roadmap for Photovoltaic (ITRPV), Eleventh edition, 2020.

[3] R. Witteck, B. Veith-Wolf, H. Schulte-Huxel, et al. "UV-induced degradation of PERC solar modules with UV-transparent encapsulation materials", Prog. Photovolt: Res. Appl., vol. 25(6), 2017.

[4] R. Witteck, P. Jäger, M. Rudolph, et al. "UV-stable surface passivation for crystalline silicon cells in solar modules with UV light transmitting encapsulation materials", 2019 IEEE 46th PVSC, DOI: 10.1109/PVSC40753.2019.8980612.

[5] F. Ye, Y. Li, W. Deng, et al. "UV-induced degradation in multicrystalline PERC cell and module", Solar Energy, vol. 170, pp. 1009–1015, 2017.

4 Plans for Future Publications

4.1 CWRU

- Cross-Correlation of Mini- and Full-Size Modules with PERC and Al-BSF Cells in Damp Heat Exposure
- Modeling of mDH/mDH + FS Minimodules

4.2 UCF

- A Review of Manufacturing Defects, Degradation Modes, and Failure Modes in Crystalline Silicon Photovoltaics
- Characterization of Front Contact Degradation in Monocrystalline and Multicrystalline Silicon Photovoltaic Modules Under Damp Heat Conditions

5 End of Project Goals (Q12)

- $< S|R >$ *models of real-world and accelerated exposures of full-size modules*
- Achieve a predictive $R^2 > 0.9$ fit for the time-dependent $<S|R>$ piecewise linear model on test datasets for at least 3 commercially relevant (of mono- or multi-crystalline, full- or half-cell PERC, and Al-BSF as determined in BP1) full-size modules in at least 1 climate zone over 3 or more years for response features in outdoor I-V datastreams, such as P_{mp}, R_{sh}, R_s, and J_0.

- **The CSI outdoor I-V stepwise data set is the longest available collection of outdoor PERC data available. We have access to multiple cell types including multi Al-BSF, full and half cell PERC, and MBB PERC cells. This data set was the primary data source for this task. We currently have 36 months of outdoor exposure data.**

- Achieve a predictive $R^2 > 0.9$ fit for the time-dependent $<S|R>$ piecewise linear model on test datasets of the same 3+ full-size module types above in at least 2000 hours of one accelerated exposure (in addition to 2 exposures from BP1) for predicted response features in indoor I-V datastreams, such as P_{mp}, R_{sh}, R_s, and EL imaging.
- **CSI has coordinated a number of accelerated tests on full sized modules, including the initial DH and TC tests, along with more recent LID and LeTID tests and DH + ML on more recent cell types. We optimized our EL image feature extraction to improve the number of variables we used in analsyis.**

- Report rank ordering for 3+ commercially relevant module types for degradation of the chosen response features (such as P_{mp}, R_{sh}, R_s, and J_0 or EL) in outdoor and accelerated conditions.
- **We combined results seen with different packaging combinations between the indoor accelerated tests and the outdoor exposure of modules to determine the best performers. There are clear distinctions in performance between cell and packaging combinations from our mDH and mDH + FS accelerated tests. We are extending our outdoor data sources to identify more outdoor degradation features.**

- Cross-correlated outdoor and accelerated $<S|R>$ models predicting P_{mp} for these 3+ full-size module types demonstrate ¡ 10% relative error in predicting outdoor power production with time-scaled accelerated exposure models.
- **Outdoor data from CSI was used to scale the accelerated tests to determine the tests that best represent the observed outdoor degradation.**

- *Analysis of encapsulants and backsheets in mini-modules*
- Report rank ordering of 6 combinations of 3 encapsulants and 2 backsheets for reduced Al-BSF and PERC mini-modules using piecewise linear predictive $<S|R>$ models of$I$-V response features (such as P_{mp}, R_{sh}, R_s, and J_0) for at least 2 years of outdoor exposure.
- **The outdoor set of mini-modules with EVA and POE encapsulants and KPx and PPf backsheet has achieved 2.5 years of measurements. We have calculated outdoor power loss mechanisms using an outdoor $Suns$-V_{OC} analysis and PLR calculations however a consistent degradation signal was not observed in either case, indicating little to no degradation occurring in these modules. We will continue to model the response features in an attempt to identify degradation modes.**

- Using 95% confidence intervals and Z-scores for standard errors constructed from the difference between PERC and Al-BSF $<S|R>$ models for 2 years of outdoor exposure, report statistically significant differences between PERC and Al-BSF mini-modules with 6 packaging strategies and for$I$-V response features such as P_{mp}, FF, Isc, Voc.
- **As with the previous task, outdoor Sun-V_{OC} loss mechanisms from the SDLE mini-modules are compared to determine any differences in performance between them.**

- Cross-correlated outdoor and accelerated P_{mp} $<S|R>$ models for PERC and Al-BSF mini-modules with 3+ packaging strategies demonstrate $<$ 10% relative error in predicting outdoor power production with time-scaled accelerated exposure models.
- **We will be able to scale our indoor accelerated tests with the measured outdoor data from the mini-modules, as we have started to do with the full sized modules. The first exposures of focus will be the mDH + FS exposure as it includes light dose similar to outdoor exposure.**

- *Characterization and inferential $<S|M|R>$ network modeling*
- Incorporate up to 6+ mechanistic variables from different characterization methods into $<S|M|R>$ inferential models and report rank order of all observed degradation modes according to contribution to power loss for 4+ types of Al-BSF and PERC mini-modules exposed outdoors for at least 2 years.
- **Applying the $Suns$-V_{OC} method to the outdoor data will allow us to extract degradation features through voltage tracking of the mini-modules to be compared with the measured I-V curves.**

- Using 95% confidence intervals and Z-scores for standard errors constructed from the difference between 4+ Al-BSF and PERC module types in 2+ years of outdoor exposures, report statistically significant differences between these mini-module types for dominant degradation modes to identify unique degradation mechanisms for each module type according to packaging type.
- **We reported degradation rates in QPI 3.3. We have have also I-V features in the analysis.**

- *Publish at least one additional peer-reviewed publication about dominant degradation modes and pathways to lower degradation rates for commercially relevant Al-BSF and PERC module architectures.*
- **We are currently working on several manuscripts using PERC and Al-BSF data from this project to determine observed differences between multi and monocrystalline cells, as well as PERC and Al-BSF.**

6 Publications/Presentations:

UConn

- Photovoltaic Tomography (MMC, Manchester, UK, 2017)
- Nanoscale Performance Mapping of Photovoltaic Properties (Lancaster University, 2017)

- PV performance mapping (U. Florida seminar, 2018)
- CT-AFM: Nanoscale Tomography of Materials Properties (IFAAP, Hiroshima, 2018)
- PVSC-46 talk and Proceedings: "Open Circuit Voltages for PERC Local Back Surface Fields Directly Resolved at the Nanoscale" Alexandra Longacre, Michael Martin, Eric Schneller, Alan J. Curran, Menghong Wang, Jing Sun, Jianfang Dai, Laura S. Bruckman, Jean-Nicolas Jaubert, Kristopher O. Davis, Jennifer L. Braid, Roger H. French, Bryan D. Huey
- Bryan D. Huey, Nanoscale and 3-D Performance of Photovoltaics, PacRim13 invited talk, Okinawa, Japan, 2019.
- Bryan D. Huey, Nanoscale Functional and Photovoltaic Property Mapping, University of Geneva invited seminar, Switzerland, 2019.
- B. D. Huey, "Nanoscale 2-Dimensional and Tomographic Photovoltaic Property Mapping," invited talk, Miasole, Santa Clara, CA, 8/7/19.
- Spectrolab: B. D. Huey, "Nanoscale and Nanovolumetric PV Performance Mapping," invited talk, Spectrolab, Sylmar, CA, 10/25/19.
- Longacre, A., Martin, M., Moran, T. et al. Direct nanoscale mapping of open circuit voltages at local back surface fields for PERC solar cells. J Mater Sci 55, 11501–11511 (2020). https://doi.org/10.1007/s10853-020-04736-x

UCF

- PVSC-46 talk and Proceedings: "Performance Evaluation of Commercially Relevant p-Type Silicon Cell Architectures" Eric Schneller, Mohammad Jobayer Hossain, Rafaela Frota, Alan J. Curran, Menghong Wang, Jean-Nicolas Jaubert, Jennifer L. Braid, Roger H. French, Kristopher O. Davis
- Schneller EJ, Hossain MJ, Frota R, Iqbal N, Colvin D, Curran AJ, Wang M, Braid JL, Bruckman LS, French RH, Huey BD, Jaubert JN, Davis KO. Spatially Resolved Characterization of Optical and Recombination Losses for Different Industrial Silicon Solar Cell Architectures. International Journal of Modern Physics B. Accepted with revisions.

CWRU

- PVPMC-9: "Insights into PERC Cell and Module Lifetime Performance from Modeling I-V, $Suns$-V_{oc}, and Advanced Characterization Data" Jennifer L. Braid, Justin S. Fada, Trey D. Wager, Xuan Ma, Roger H. French, December 2017
- CWRU Research ShowCASE: "Investigating Degradation of PERC Solar Cells Through Microwave Photoconductive Decay" Trey D. Wager, Jennifer L. Braid, Roger H. French, April 2018

- WCPEC-7 Poster and Proceedings: "EL and I-V Correlation for Degradation of PERC vs. Al-BSF Commercial Modules in Accelerated Exposures" Jennifer L. Braid, Alan J. Curran, Jing Sun, Eric J. Schneller, Justin S. Fada, Jiqi Liu, Menghong Wang, Alexandra J. Longacre, Jeff Dai, Bryan D. Huey, Kristopher O. Davis, Jean-Nicholas Jaubert, Laura S. Bruckman, Roger H. French, June 2018
- WCPEC-7 Poster and Proceedings: "Initial Stability of PERC vs Al-BSF Cells" Jennifer L. Braid, Trey D. Wager, Alexandra J. Longacre, Bryan D. Huey, Roger H. French, June 2018
- CWRU Summer Undergraduate Research in Energy and Sustainability (SURES) Presentation: "Initial Degradation of AL-BSF vs PERC Photovoltaics Cells with Different Packaging Strategies" Arushi Pradhan, July 2018
- PVSC-46 talk and Proceedings: "Degradation of PERC and Al-BSF Photovoltaic Cells with Differentiated Minimodule Packaging Under Damp Heat Exposure" Menghong Wang, Alan J. Curran, Eric Schneller, Jing Sun, Jianfang Dai, Arushi Pradhan, Shiyi Qin, Erika L. Anderson, Sean M. Morrison, Muhammad Syaheen Sazally, Laura S. Bruckman, Kristopher O. Davis, Bryan D. Huey, Jean-Nicolas Jaubert, Jennifer L. Braid, Roger H. French
- PVSC-46 poster and Proceedings: "Accurate linear extraction of ideality factor, series and shunt resistance from I-V curves" Jennifer L. Braid
- PVSC-46 poster and Proceedings(Best poster award): "Performance Loss Rate Consistency and Uncertainty Across Multiple Methods and Filtering Criteria" Alan J. Curran, Christian B. Jones, Sascha Lindig, Joshua Stein, David Moser, Roger H. French
- PVSC-46 poster and Proceedings: "Performance Loss Rates of PV systems of Task 13 database" Sascha Lindig, David Moser, Alan Curran, Roger French
- CWRU SURES Poster: "Optimizing Lamination Cycle for EVA and POE", Muhammad Syaheen Sazally, July 2018
- Performance & Reliability of PERC Modules: Cell and Packaging Architectures Workshop March 21st, 2019 Online Webinar
- Tohoku/CWRU Data Science Symposium (August 2019)
  Comparative Connector Degradation Analysis of Al-BSF and Monofacial PERC Modules in Modified Damp Heat Exposure
  Evaluation of Solar Plant Performance Loss Rate Calculation Methods
- PVSC-47 talk and proceedings: "Degradation of bifacial PERC and Al-BSF cell minimodules with white and clear encapsulant combinations in modified damp heat", Alan J. Curran, Menghong Wang, Jennifer L. Braid, Krisopher O. Davis, Bryan D. Huey, Thomas Moran, Dylan Colvin, Brent Brownell, Nafis Iqbal, Carolina Whitaker, Jean-Nicolas Jaubert, Laura S. Bruckman, Roger H. French
- PVSC-47 talk and proceedings: "PVplr: R Package Implementation for Diverse Time-series Degradation Analysis ", Alan J. Curran, Tyler L. Burleyson, Sascha Lindig, David Moser, Joshua Stein, Laura S. Bruckman, Roger H. French

- M. Wang, T. J. Burleyson, J. Liu, A. J. Curran, E. J. Schneller, K. O. Davis, J. L. Braid, R. H. French, SunsVoc: Constructing Suns-Voc from Outdoor Time-series I-V Curves, 2020. `https://CRAN.R-project.org/package=SunsVoc`.

- Alan Curran, Tyler Burleyson, Sascha Lindig, David Moser ORCID, Roger French, PVplr: Performance Loss Rate Analysis Pipeline, 2020 `https://cran.r-project.org/package=PVplr`

- Sascha Lindig, David Moser, Alan J. Curran, Kunal Rath, Arash Khalilnejad, Roger H. French, Magnus Herz, Björn Müller, George Makrides, Mauricio Richter, Julián Ascencio-Vásquez, Mike van Iseghem, Mohammed Meftah, Dirk C. Jordan, Chris Deline, Wilfried van Sark, Joshua S. Stein, Marios Theristis, Bennet Meyers, Franz Baumgartner, Luo Wei, "INTERNATIONAL COLLABORATION FRAMEWORK FOR THE CALCULATION OF PERFORMANCE LOSS RATES: DATA QUALITY, BENCHMARKS AND TRENDS (Towards a uniform methodology)", Accepted for publication in Progress in Photovoltaics: Research and Applications.

7 References

*

[1] A. Curran, T. Burleyson, S. Lindig, D. Moser, R. French, PVplr: Performance Loss Rate Analysis Pipeline, r package version 0.1.0 (2020).
URL `https://CRAN.R-project.org/package=PVplr`

[2] M. Wang, Degradation of photovoltaic packaging materials and power output of photovoltaic systems: Scaling up materials science with data science, Ph.D. thesis, Case Western Reserve University (2020).

[3] A. Al-Ashouri, E. Köhnen, B. Li, A. Magomedov, H. Hempel, P. Caprioglio, J. A. Marquez, A. B. M. Vilches, E. Kasparavicius, J. A. Smith, et al., Monolithic perovskite/silicon tandem solar cell with $>$ 29% efficiency by enhanced hole extraction, Science 370 (6522) (2020) 1300–1309.

[4] Y. Rong, Y. Hu, A. Mei, H. Tan, M. I. Saidaminov, S. I. Seok, M. D. McGehee, E. H. Sargent, H. Han, Challenges for commercializing perovskite solar cells, Science 361 (6408) (2018).

[5] J. Song, Y. Zhou, N. P. Padture, B. D. Huey, Anomalous 3d nanoscale photoconduction in hybrid perovskite semiconductors revealed by tomographic atomic force microscopy, Nature communications 11 (1) (2020) 1–9.

[6] F. Bella, G. Griffini, J.-P. Correa-Baena, G. Saracco, M. Grätzel, A. Hagfeldt, S. Turri, C. Gerbaldi, Improving efficiency and stability of perovskite solar cells with photocurable fluoropolymers, Science 354 (6309) (2016) 203–206.

8 Acknowledgment

This material is based upon work supported by the U.S. Department of Energy's Office of Energy Efficiency and Renewable Energy (EERE) under Solar Energy Technologies Office (SETO) Agreement Number DE-EE-0008172.

9 Disclaimer

Appendix

Issues, Risks, and Mitigation:

We anticipate no critical problems or delays at this time.

Changes in Approach:

We have not instituted any changes to our approach at this stage of the project.

Key Personnel

:

Recipient and Principal Investigator Disclosures:

There are no Recipient or Principal Investigator Disclosures at this time. None of the sponsored persons or entities have been debarred, suspended, or found insolvent. Similarly, there have been no fraud convictions, violations of export control laws and regulations, or violations of the Drug-Free Workplace Act of 1988 to report.

Conflicts of Interests Within Project Team:

There are no Conflicts of Interest within the Project Team to report at this time.

Performance of Work in the United States:

There is no work funded under this award being performed outside the United States.